Balancing of mitochondrial translation through METTL8-mediated m^{3}C modification of mitochondrial tRNAs

Eva Schöller[1], James Marks[2], Virginie Marchand[3], Astrid Bruckmann[1], Christopher A. Powell[4], Markus Reichold[5], Christian Daniel Mutti[4], Katja Dettmer[6], Regina Feederle[7], Stefan Hüttelmaier[8], Mark Helm[9], Peter Oefner[6], Michal Minczuk[4], Yuri Motorin[3,10], Markus Hafner[2] & Gunter Meister[1, 11]

[1] Regensburg Center for Biochemistry (RCB), Laboratory for RNA Biology, University of Regensburg, 93053, Regensburg, Germany

[2] RNA Molecular Biology Group, Laboratory of Muscle Stem Cells and Gene Regulation, National Institute of Arthritis and Musculoskeletal and Skin Diseases, Bethesda, MD, 20892, USA

[3] Université de Lorraine, CNRS, INSERM, UMS2008/US40 IBSLor, EpiRNA-Seq Core facility, F-54000 Nancy, France

[4] Medical Research Council Mitochondrial Biology Unit, University of Cambridge, Hills Road, Cambridge, CB2 0XY, UK

[5] Medical Cell Biology, Institute of Physiology, University of Regensburg, 93053, Regensburg, Germany

[6] Institute of Functional Genomics, University of Regensburg, 93053, Regensburg, Germany

[7] Monoclonal Antibody Core Facility, Institute for Diabetes and Obesity, Helmholtz-Zentrum München, German Research Center for Environmental Health, 85764 Neuherberg, Germany

[8] Institute of Molecular Medicine, Section for Molecular Cell Biology, Faculty of Medicine, Martin-Luther-University Halle-Wittenberg, 06120, Halle, Germany

[9] Institute of Pharmacy and Biochemistry, Johannes Gutenberg-University, Staudingerweg 5, D-55128 Mainz, Germany

[10] Université de Lorraine, CNRS, UMR7365 IMoPA, F-54000 Nancy, France

[11] lead contact

Correspondence: Gunter Meister (gunter.meister@ur.de)

Key words: m^3C, METTL8, mt-tRNA, RNA modification, translation

Abstract

Mitochondria contain a specific translation machinery for the synthesis of mitochondria-encoded respiratory chain components. Mitochondrial tRNAs (mt-tRNAs) are also generated from the mitochondrial DNA and, similar to their cytoplasmic counterparts, are post-transcriptionally modified. Here, we find that the RNA methyltransferase METTL8, is a mitochondrial protein that facilitates m^3C methylation at position C_{32} of mt-tRNA$^{Ser(UCN)}$ and mt-tRNA^{Thr}. METTL8 knock-out cells show a reduction in respiratory chain activity, while over-expression increases activity. In pancreatic cancer, METTL8 levels are high, which correlates with lower patient survival and an enhanced respiratory chain activity. Mitochondrial ribosome profiling uncovered mitoribosome stalling on mt-tRNA$^{Ser(UCN)}$- and mt-tRNA^{Thr}-dependent codons. Further analysis of the respiratory chain complexes using mass spectrometry revealed reduced incorporation of the mitochondrially encoded proteins ND6 and ND1 into complex I. The well-balanced translation of mt-tRNA$^{Ser(UCN)}$- and mt-tRNA^{Thr}-dependent codons through METTL8-mediated m^3C_{32} methylation might therefore facilitate the optimal composition and function of the mitochondrial respiratory chain.

Introduction

RNA modification is a conserved and very common phenomenon that is found on almost all RNA species. Non-coding RNAs such as ribosomal RNAs (rRNAs) and transfer RNAs (tRNAs) are heavily modified leading to characteristic RNA structures and functions. tRNAs are equipped with amino acids (aminoacylated) and the anticodon information to decode the genetic information on the mRNA. They interact with the ribosome as well as the codons and many modifications are important for these interactions. For example, the anticodon can carry many different chemical alterations at the wobble position 34. This allows for wobble pairing and an increase of the codon spectrum and thus the decoding potential of a particular tRNA. In addition, the anticodon arm is also heavily modified at regions flanking the anticodon which is,

for example, important for proper ribosome binding and progression through the translation cycle (Suzuki, 2021). Such modifications can lead to structural arrangements within the anticodon arm that are important for this process. Modifications in other parts of the tRNA are often required for correct aminoacylation or adapting a specific secondary structure, which is needed for specific aspects of the tRNA life cycle. This is not only observed for human cytoplasmic tRNAs but also for mt-tRNAs, which nevertheless contain fewer modifications. The 22 human mt-tRNAs contain 18 types of chemical modifications that have been mapped to 137 positions (Suzuki et al., 2020). All modifications are generated by specialized, nuclear-encoded enzymes and many mitochondrial modification pathways are affected in human diseases such as encephalopathy or the complex mitochondria-related diseases MELAS and MERRF (Bohnsack and Sloan, 2018b; Kazuhito and Wei, 2020) (Suzuki et al., 2011).

More recently, RNA modifications have also been identified on human mRNAs. Besides the well-known cap structure where 7-methylguanosine (m^7G) is added, N^6-methyladenosine (m^6A) is the most abundant modified nucleotide on mRNA (Desrosiers et al., 1974; Dominissini et al., 2012; Meyer et al., 2012) affecting alternative splicing, mRNA export and localization, translation or mRNA stability (Balacco and Soller, 2019) (Ke et al., 2017; Knuckles et al., 2017; Lee et al., 2020; Slobodin et al., 2017; Zhou et al., 2019).

The m^6A methylation mark is catalyzed by a specific writer complex composed of the enzyme methyltransferase-like 3 (METTL3) and its binding partner METTL14 (Liu et al., 2014). Within this tight heterodimeric complex, both proteins form the catalytic center that recognizes the well-known RRACH (R=G/A; H=A/C/U) motif for m^6A methylation (Scholler et al., 2018; Sledz and Jinek, 2016; Wang et al., 2016a; Wang et al., 2016b).

METTL3 and METTL14 are members of a large family of methyltransferases and many of them have recently been associated with RNA or DNA methylation. The closest relative is METTL4, which has been implicated in m^6A modification on DNA (m^6dA) (Hao et al., 2020; Kweon et al., 2019) although quantitative LC-MS experiments did not find m^6dA at least in

DNA from mouse tissues (Schiffers et al., 2017). It also generates m^6A on small nuclear RNAs (snRNAs) that are additionally methylated at the 2' position of the ribose to generate m^6Am (Chen et al., 2020) (Goh et al., 2020). METTL16 and METTL5 catalyze the formation of m^6A as well. While METTL5 generates m^6A on the 18S rRNA at position A1832 (Ignatova et al., 2020b) (van Tran et al., 2019), METTL16 modifies one specific A of the U6 snRNA (Pendleton et al., 2017; Warda et al., 2017). Furthermore, METTL16 recognizes and modifies a distinct structural element in the SAM synthetase MAT2A (Doxtader et al., 2018) (Mendel et al., 2018). Another methyltransferase acting on RNA is METTL1, which generates m^7G modifications on a variety of different substrates including tRNAs, microRNA precursors and mRNAs (Alexandrov et al., 2002; Lin et al., 2018; Zhang et al., 2019). METTL15 localizes to mitochondria and introduces N^4-methylcytidine (m^4C) into mitochondrial 12S rRNA, which affects proper biogenesis of mitochondrial ribosomes (Van Haute et al., 2019).

METTL2, 6 and 8 catalyze the formation of 3-methylcytidine (m^3C) in tRNAs and mRNAs (Xu et al., 2017). METTL2 and 6 target cytoplasmic tRNAs and modify them at distinct positions. For example, METTL6 methylates tRNAs at C_{32} and is important for pluripotency and tumor cell growth (Ignatova et al., 2020a). METTL8 may not affect tRNAs but has been suggested to add m^3C modifications to cellular mRNAs. Furthermore, METTL8 seems to affect R-loop formation at ribosomal DNA (rDNA) loci (Zhang et al., 2020). R-loops are DNA-RNA hybrids at active transcription sites but whether METTL8 directly modifies the nascent RNA within these structures remains unclear.

Since METTL3 and METTL14 form a tight complex, which is important for catalytic activity, it is possible that other METTL proteins are subunits of larger complexes as well. A comprehensive mass spectrometry study revealed, however, that most of the tested METTL proteins are most likely not organized in stable complexes but may function as monomeric subunits, with only METTL7, 8 and 9 seeming to engage in stable interactions with other

proteins. It is however, possible that interactions are restricted to specific compartments, tissues or developmental stages that have not been investigated so far (Ignatova et al., 2019).

Here, we have assessed the biochemical mechanisms and molecular functions of METTL8 in human cells. In contrast to recent reports, we did not find evidence for METTL8-mediated mRNA modification. Instead, we found that METTL8 is a mitochondrial protein that targets m^3C_{32} modification of mt-tRNA$^{Ser(UCN)}$ and mt-tRNA^{Thr}. METTL8 knock-out (KO) leads to unmodified tRNAs and compromized respiratory chain activity. Using ribosome profiling in KO and METTL8 overexpressing cells, we found that ribosomes are stalled specifically at mt-tRNA$^{Ser(UCN)}$ and mt-tRNA^{Thr} codons and mass spectrometry identified that the mitochondrial proteins ND1 and ND6 are affected most by METTL8 activity. Finally, METTL8 over-expression is observed in highly aggressive pancreatic cancer cells, which is accompanied by a markedly enhanced respiratory chain activity. Such an METTL8 addiction of pancreatic cancer cells might be a valuable novel target for RNA therapeutics.

Results

METTL8 is a mitochondrial protein

Previous research has suggested that human METTL8 modifies mRNAs or potentially R-loops, which would occur in the cytoplasm or in the nucleus (Xu et al., 2017) (Zhang et al., 2020). In order to better understand METTL8 function, we initiated our study by performing localization experiments (Figure 1). We fused FLAG/HA (F/H)-tags to the C-terminus of METTL8 and performed immunofluorescence experiments (Figure 1A). We probed the METTL8-F/H expressing cells either with antibodies against the FLAG-tag (Top panels, right) or a newly generated monoclonal antibody against METTL8 (Top panels, left; suppl. Figure 1A for METTL8 antibody validation). Unexpectedly, we did not observe nuclear staining but detected a granular cytoplasmic signal in both experiments. The characteristic cytoplasmic signal suggested a potential mitochondrial localization and thus we co-stained METTL8-FLAG- or -

GFP expressing cells either with antibodies against the outer membrane protein TOMM20 (Figure 1B, upper panels) or MitoTracker, a reagent that specifically localizes to mitochondria (lower panels). In both experiments, METTL8 co-localized with mitochondrial markers supporting the mitochondrial localization of METTL8 in fluorescence experiments. Similar results were obtained with HeLa cells (suppl. Figure 1B). To further corroborate mitochondrial localization, we performed biochemical fractionation experiments (Figure 1C). We purified mitochondria through several steps and performed western blotting against the nuclear marker protein NRB54, the cytoplasmic marker ACTIN and the mitochondrial inner membrane marker TIMM44. Endogenous METTL8 was enriched by immunoprecipitation prior to western blotting to increase signal intensities. While METTL8 was not detectable in the debris (which also contains nuclei) or the cytoplasmic fractions, it was clearly detectable in the mitochondrial fraction (Figure 1C). To exclude that METTL8 associates specifically or unspecifically with the surface of mitochondria we treated the purified mitochondria with proteinase K (PK). This treatment had no effect on the METTL8 signal in the mitochondrial fraction demonstrating that METTL8 is a mitochondrial protein.

Mitochondrial localization is frequently mediated by mitochondrial targeting signals (MTS) and indeed we found a potential motif at the very N terminus of METTL8 (Figure 1D). Of note, this motif is not present in the closely related proteins METTL2A, 2B and 6 (suppl. Figure 1C). To directly test the functionality of this targeting motif, we mutated several key isoleucine (Ile) residues to Glutamine (Gln) (Figure 1D). The GFP-tagged METTL8 mutants were transfected into HEK 293 cells and co-stained with MitoTracker (Figure 1E). Mutation of the first Ile (Ile^{4}) still resulted in mitochondrial localization but a mild diffuse cytoplasmic signal can also be detected (panels I). Double mutation of Ile4 and 9 ($Ile^{4,9}$) led to a clear cytoplasmic signal (panels II) confirming that the targeting signal is required for mitochondrial localization. Biochemical fractionations fully confirmed our immunofluorescence observations (Figure 1F). Of note, a triple mutation including Ile4,9 and Leu12 resulted in a complete mis-localization to

nucleoli (Figure 1E, panel III) followed by rapid cell death (IV). Thus, it is possible that nucleolar localization that has been reported before could be due to N terminal tagging of METTL8, which might interfere with mitochondrial targeting (Zhang et al., 2020). Moreover, it is also conceivable that METTL8 isoforms exist that lack the MTS and thus may have other cellular functions. However, scrutinizing known mouse isoforms detected a potential MTS in all isoforms arguing against mitochondria-independent functions (suppl. Figure 1D). Taken together, we found that the RNA methyltransferase METTL8 is a mitochondrial protein.

METTL8 binds a subset of mitochondrial tRNAs but is dispensable for their aminoacylation

Since METTL8 localizes to mitochondria, we examined whether METTL8 associates with mt-RNAs in human cells. First, we generated METTL8 KO HEK 293 cells using CRISPR and confirmed successful KO by western blotting against endogenous METTL8 (Figure 2A). These cells served as specificity control in our immunoprecipitations. We next immunoprecipitated METTL8 from HEK 293 cells and analyzed co-isolated mt-mRNAs by qPCR (Figure 2B). None of the mt-mRNA transcripts were specifically enriched indicating that METTL8 does not stably associate with mt-mRNAs. Since the closely related methyltransferases METTL6 and METTL2 act on tRNAs (Xu et al., 2017), we next investigated binding of METTL8 to mt-tRNAs. (Figure 2C). Using Northern blotting, we observed that mt-tRNA$^{Ser(UCN)}$, mt-tRNA^{Arg}, mt-tRNA^{Thr} and mt-tRNA^{Trp} associated with overexpressed METTL8-F/H while all other mitochondrial tRNAs did not (Figure 2B and data not shown). Furthermore, mt-tRNA$^{Ser(UCN)}$ and mt-tRNA^{Arg} were also efficiently co-immunoprecipitated with endogenous METTL8 while no signal is detected in METTL8 KO cells indicating highly specific binding signals. Notably, mt-tRNA^{Thr} appears to be low abundant, which is most likely the reason for the weak signal in METTL8 immunoprecipitates. Furthermore, it is the only mitochondrial tRNA that is up regulated in METTL8 KO cells as evident from the Northern blot input samples suggesting

additional METTL8 have effects on this particular mt-tRNA (Figure 2C). To further corroborate these observations, we performed Northern blots on increasing amounts of total RNA from WT METTL8, KO and over expressing HEK 293 cells (Figure 2D). Consistently, mt-tRNA^{Thr} levels depend on the expression status of METTL8. As a further control, we expressed F/H-METTL2, which is known to modify the cytoplasmic tRNA$^{Thr(AGT)}$ (Figure 2E). Anti-FLAG-METTL2 immunoprecipitation revealed that tRNA$^{Thr(AGT)}$ is efficiently enriched, while mt-tRNA^{Thr} does not bind to METTL2 indicating that the observed METTL8 interactions are highly specific.

Under steady-state conditions, most cellular tRNAs are covalently bound to amino acids. We performed aminoacylation assays using acid gels to analyze whether METTL8 function is required for aminoacylation of its mt-tRNA targets (Figure 2F). Mitochondrial RNA was isolated from WT or METTL8 KO HEK 293 cells and the aminoacylation status was measured using acid gelelectrophoresis (Varshney et al., 1991). Deacylated mt-tRNAs migrate faster in acid gels and can thus be easily detected. Both in WT cells and in three independent METTL8 KO clones, the METTL8-associated mt-tRNAs carry amino acids indicating that METTL8 is dispensable for mt-tRNA aminoacylation.

Reduced m^3C_{32} mt-tRNA modification in METTL8 KO cells

It has been reported that METTL8 generates m^3C in mRNAs (Xu et al., 2017). Since our data point towards a mitochondrial function, we performed an unbiased m^3C screening approach using AlkAniline-Seq, which allows for the genome-wide detection of m^3C and m^7G modifications (suppl. Figure 2A for a schematic overview) (Marchand et al., 2018). Both mt-tRNA$^{Ser(UCN)}$ and mt-tRNA^{Thr} were reported to contain an m^3C at position 32 (Suzuki et al., 2011; Suzuki and Suzuki, 2014; Suzuki et al., 2020). Indeed, AlkAniline-Seq revealed that m^3C_{32} is lost on both mt-tRNAs in METTL8 KO cells while it can be readily detected in WT HEK 293 cells (Figure 3A). m^3C modification patterns of the cytoplasmic tRNA$^{Ser(UGA/GCU)}$ or

the tRNA^{Thr} are unchanged in METTL8 KO cells indicating that the effect is specific and restricted to mitochondrial tRNAs (suppl. Figure 2B). Notably, mt-tRNA^{Arg}, which was bound to METTL8 in our interaction assays (Figure 2C) does not contain a C at position 32 but instead carries a U. Consequently, we did not observe any changes in METTL8 KO cells (Figure 3A). Similarly, although mt-tRNA^{Trp}, which showed some binding to METTL8 (Figure 2C) carries a C at position 32, this C has not been reported to be methylated at all (Suzuki et al., 2011; Suzuki and Suzuki, 2014) and, correspondingly, we neither observed a modified C_{32} nor any changes between WT and METTL8 KO cells. We confirmed our AlkAniline-Seq results in HAP-1 cells using classical primer extension experiments (suppl. Figure 2C and D). Taken together, mt-tRNAs that contain m^3C_{32} are unmodified in METTL8 KO cells indicating that METTL8 modifies these two distinct sites within the mitochondrial tRNA population.

METTL8-mediated m^3C_{32} methylation is linked to isopentenylation of A_{37}

To unravel the biochemical principles underlying METTL8 activity, we set out to reconstitute mt-tRNA C_{32} methylation *in vitro*. We expressed METTL8 and purified it from bacterial lysates (Figure 3B and suppl. Figure 2E). C_{32} is located in the anticodon arm of mt-tRNA$^{Ser(UCN)}$ and mt-tRNA^{Thr} and thus we designed an RNA substrate resembling the anticodon arm of mt-tRNA$^{Ser(UCN)}$ (Figure 3B). Recombinant METTL8 was subsequently incubated with the RNA substrate and radioactively labeled S-adenosyl-methionine as methyl donor. However, we did not observe METTL8 activity under these conditions (Figure 3C, (I) and 3D). Interestingly, mt-tRNA$^{Ser(UCN)}$ contains an isopentenylated A (i^6A) at position 37 (Suzuki et al., 2011; Suzuki and Suzuki, 2014) and thus we reasoned that METTL8 may require prior i^6A_{37} modification as has been observed for yeast cytoplasmic tRNAs (Arimbasseri et al., 2016) (Han and Phizicky, 2018). We expressed TRIT1, the human mitochondrial i^6A modifying enzyme (Lamichhane et al., 2013), in bacteria and purified the recombinant protein (Figure 3B, suppl. Figure 2E). Strikingly, when the anticodon RNA substrate was pre-incubated with TRIT1 in an

isopentenylation reaction, it became an efficient substrate for METTL8 and m^3C_{32} was efficiently methylated (Figure 3C, (II) and 3D). In a control reaction, where C_{32} was mutated to G_{32}, no METTL8 activity was detected even in the presence of i^6A_{37} (Figure 3C, (III) and 3D). Similarly, a negative control substrate did also not result in detectible activity (ctrl.). Therefore, our biochemical reconstitution revealed that METTL8 requires prior TRIT1 activity presumably to generate the i^6A_{37} modification in order to set the m^3C_{32} mark on the mt-$tRNA^{Ser(UCN)}$.

To further define the catalytic activity of METTL8 and to control for specificity in our *in vitro* measurements, we mutated and thus inactivated METTL8. Since structural information for METTL8 is not available, we aligned METTL2, 6 and 8 and predicted D230 within the AdoMet domain as residue potentially relevant for catalysis (Figure 3B and 3E). We mutated D230 to Alanine (D230A), expressed it in HEK 293 cells and performed methylation assays with the immunoprecipitates. When the mutated METTL8 variant was used, m^3C_{32} methylation was not detectable (Figure 3F). Therefore, the observed activity is METTL8-specific and D230A is a critical amino acid that is required for the enzymatic reaction.

Reduced respiratory chain activity in METTL8-deficient cells

Mitochondria host the respiratory chain and provide most of the cellular energy under aerobic conditions. Since several components of the respiratory chain are translated from mitochondrial transcripts and METTL8 is important for mt-tRNA modification, we hypothesized that METTL8 deletion might affect respiratory chain activity. For a first glimpse on metabolism, we compared intra- (Figure 4A) and extracellular (Figure 4B) metabolite levels using gas chromatography-mass spectrometry. Although statistically not significant, we observed increased intracellular succinate levels in the METTL8 KO cells (Figure 4A). Extracellular pyruvate, lactate and glucose levels, however, remain unchanged (Figure 4B). These data would be consistent with a model, in which succinate accumulates potentially due to an impaired

respiratory chain function. Increased succinate levels might suggest a compromised complex II activity of the respiratory chain downstream of the tricarboxylic acid (TCA) cycle. Negative feedback mechanisms may lead to an overall reduced glucose metabolism.

To directly test respiratory chain activity, we performed high-resolution respirometry (Oroboros-2k) and assessed key features of respiratory chain activity (Figure 4C). Parameters such as routine activity, OXPHOS capacity, electron transport system (ETS) and the leak state were clearly reduced in METTL8 KO cells (Figure 4C). These general respiratory chain impairments can be linked to reduced complex I and II (CI, CII) activities (Figure 4C).

We next investigated whether the reduced respiratory chain activity is caused by a general METTL8 loss or the lack of its enzymatic activity and thus loss of m^3C_{32} modification of mt-tRNAs. We rescued METTL8 KO HEK 293 cells either with WT METTL8 or with its catalytic mutant (D230A) and repeated the high-resolution respiratory experiments (Figure 4D). We directly compared rescue activity of WT METTL8 and METTL8-D230A and found that WT METTL8 rescued routine activity, OXPHOS capacity, electron transport system (ETS) and the leak state efficiently, while the catalytic METTL8 mutant rescued OXPHOS capacity and ETS to a much lesser degree. Effects on routine activity and leak state did not reach statistical significance (Figure 4D). Differences between WT and mutant METTL8 rescue experiments were even more apparent when complex I and II activities were analyzed (Figure 4D). Therefore, we conclude that the loss of METTL8 activity and thus the loss of m^3C_{32} modification of mt-$tRNA^{Ser(UCN)}$ and mt-$tRNA^{Thr}$ affects specific activities of the respiratory chain.

METTL8 expression correlates with cell growth and patient survival in pancreatic cancer

Our observations that METTL8 is important for proper respiratory chain function together with previous findings that METTL8 is mis-expressed in several cancers (Begik et al., 2020; Zhang et al., 2020), prompted us to deeper investigate a potential link between METTL8 and cancer.

We first assessed whether METTL8 KO affects cell proliferation in HEK 293 cells (Figure 5A). Although statistically not significant, a potential grow defect can be observed in two KO HEK 293 cell clones (Figure 5A, upper panel). WT METTL8 rescued the growth phenotype more effectively than the catalytic mutant (D230A) (lower panel) highlighting the importance of the catalytic activity for the phenotype. We next analyzed publicly available gene expression data from cancer samples or normal tissues (Database: TCGA, Figure 5B). In agreement with previous observations (Begik et al., 2020), METTL8 is up-regulated in diffuse large B cell carcinoma (DLBC), glioblastoma (GBM), low grade glioma (LGG), lung squamous cell carcinoma (LUSC), pancreatic adenocarcinoma (PAAD), stomach adenocarcinoma (STAD) and thyroid carcinoma (THYM) (Figure 5B, C). Since mis-regulation is not necessarily relevant for pathogenies, we asked whether METTL8 up-regulation also translates into patient survival rates and generated Kaplan-Meier curves based on TCGA data (Figure 5D). In six of the seven cancer types, METTL8 up-regulation is not correlated with overall patient survival. In contrast, in the highly aggressive pancreatic cancer, high METTL8 levels correlate with significantly lower survival rates suggesting that increased METTL8 levels could be relevant for pancreatic cancer pathology (Figure 5D).

To further corroborate this model, we knocked out METTL8 in the pancreatic cancer cell line PANC-1 (Figure 5E), which resulted in a much stronger delay in cell growth compared to HEK 293 cells (Figure 5F, left panel). Furthermore, over-expression of METTL8 in HEK 293 cells, which mirrors the conditions in PAAD and the PANC-1 cell line, strongly accelerated cell proliferation (Figure 5F, right panel). Our data therefore suggest that METTL8 may serve as bottleneck for cell proliferation, which might be specifically important for rapidly growing pancreatic cancer cells.

Increased mt-tRNA$^{Ser(UCN)}$ m^{3}C$_{32}$ methylation and respiratory chain activity in the pancreas carcinoma cell line PANC-1

To further assess the role of METTL8 in pancreatic cancer, we analyzed the mt-tRNA$^{Ser(UCN)}$ mt-tRNA^{Thr} methylation status in the PAAD-derived cell lines PANC-1 and CAPAN-1 and compared it with HEK293 cells using AlkAniline-Seq (Figure 6A). The signal for the methylation status of mt-tRNA^{Thr} was > 750U indicating that the mt-tRNA^{Thr} population is most likely fully methylated in all three cell lines (panels I-III). Interestingly, only minor fraction (about 5-10%) of the mt-tRNA$^{Ser(UCN)}$ population appears to be methylated in HEK293 cells, while the bulk of mt-tRNA$^{Ser(UCN)}$ remains unmethylated at position C$_{32}$ (suggested by a signal of only about 150U, panel IV). Strikingly, mt-tRNA$^{Ser(UCN)}$ methylation is at least 2.5-fold higher in PANC-1 cells (380U, please note that the calibration curve is non-linear for AlkAniline-Seq signals (Marchand et al., 2018)), which would be in line with increased METTL8 activity in these cells (panel V and Figure 6B). However, when assessing the second PAAD-derived cell line CAPAN-1, mt-tRNA$^{Ser(UCN)}$ C$_{32}$ methylation was as low as in HEK 293 cells (panel VI). These results were puzzling since both PANC-1 and CAPAN-1 cells derive from PAAD. Because we reasoned that METTL8 levels correlate with the tRNA methylation status, we assessed METTL8 protein levels by western blotting (Figure 6B). In agreement with our model, METTL8 expression levels in CAPAN-1 cells are much lower compared to PANC-1 cells, which could readily explain the differential mt-tRNA$^{Ser(UCN)}$ C$_{32}$ methylation status between the two pancreatic cancer cell lines (Figure 6A and B). Of note, CAPAN-1 cells are derived from liver metastasis of pancreas cancer and may have adjusted METTL8 levels to specific needs during liver colonization.

To examine whether the METTL8 levels in the three cell lines also affect their respiratory chain activities, we performed Oroboros measurements and again tested a number of respiratory chain parameters (Figure 6C). We found that routine activity, OXPHOS capacity, the electron transport system (ETS) and the leak state are increased in PANC-1 cells compared to CAPAN-

1 and the non-cancer pancreas cell line A549 (Figure 6C). Moreover, PANC-1 cells possess much stronger complex I activity and also complex II activity is moderately increased (Figure 6C), which is consistent with strong METTL8 up-regulation in PANC-1 cells (Figure 6D). To further test the importance of METTL8 for PANC-1 cells, we assessed respiratory chain activity under METTL8 KO conditions (Figure 6E). Consistently, all respiratory chain parameters are reduced when METTL8 is deleted (Figure 6E). In summary, our data suggest a model in which particularly PANC-1 cells might be addicted to high METTL8 levels.

We next asked whether the METTL8 effects observed in PANC-1 cells can be reconstituted in other cells lines or whether there are unknown PANC-1-specific factors besides increased METTL8 level that contribute to the enhanced activity of the respiratory chain. We therefore overexpressed METTL8 in HEK293 cells and assessed m^3C modification using AlkAniline-Seq. Overexpression of METTL8 leads to at least two-fold increase of m^3C_{32} on mt-tRNA$^{Ser(UCN)}$ (Figure 6F, lower panel) while mt-tRNA^{Thr} is not further modified since it is likely fully methylated already (Figure 6F, upper panel). Furthermore, METTL8 over-expression results in a moderate increase of the OXPHOS capacity and CI activity. Other parameters are rather unaffected (Figure 6G). Thus, mimicking METTL8 levels of PANC-1 in HEK 293 cells partially leads to similar phenotypes, which supports our hypothesis that METTL8 represents a general bottleneck for respiratory chain function through mt-tRNA$^{Ser(UCN)}$ methylation.

The mt-tRNA$^{Ser(UCN)}$ m^3C_{32} status and respiratory chain composition depend on METTL8 levels

An obvious scenario would be that inefficient mt-tRNA$^{Ser(UCN)}$ methylation impacts translation of transcripts containing mt-tRNA$^{Ser(UCN)}$ codons. Since these codons appear to be randomly distributed and found in almost all mitochondrial mRNAs (suppl. Figure 3A), we performed an unbiased metabolic labeling approach (Figure 7A). HEK293, PANC1 and HAP1 cells where grown on radiolabeled methionine in the presence of emetine dihydrochloride. Under these

conditions, cytoplasmic translation is blocked while mitochondrial translation is unaffected. The 13 mitochondrial proteins can be separated by gel electrophoresis and quantified. Using this approach, we did not find considerable differences between WT and METTL8 KO cells (Figure 7A, right). Of note, not all mitochondria-encoded proteins can be efficiently detected with this method. Since we did not observe a global effect on mitochondrial translation, we analyzed respiratory chain sub-complex composition by native gel electrophoresis followed by mass spectrometry (Figure 7B). Mitochondrial proteins from WT, METTL8 KO and METTL8 overexpressing HEK 293 cells were loaded on a blue-native gel separating sub-complexes of the respiratory chain. Complexes I and II are assembled from distinct pre-formed modules (suppl. Figure 3B), which were excised from the gel, analyzed by mass spectrometry and the identified proteins compared between the investigated conditions (Figure 7B, left). A comprehensive detection of all components of the respiratory chain is challenging due to molecular weight and abundance in the native complexes, membrane association or solubility (Barros and McStay, 2020). Accordingly, we did not reliably identify all components under normal conditions (Figure 7B, right, 'HEK 293 WT' represents factors that were not detectable). Interestingly, when METTL8 was overexpressed (Figure 7B, 'METTL8 WT_{OE}'), we readily detected all components of the respiratory chain in our analysis suggesting that METTL8 levels may affect the abundance of specific components in respiratory chain assemblies. Moreover, cells in which METTL8 was deleted (Figure 7B, 'METTL8 KO'), four additional proteins were missing in our measurements (Figure 7B, highlighted in red). While two of them are nuclear encoded (NDUFA6, SDHD), ND1 and ND6 are expressed from the mitochondrial genome and are therefore candidates that could be directly affected by METTL8. Since mitochondrial translation is globally almost unchanged when METTL8 is lost (Figure 7A) and we did not find a bias for mt-$tRNA^{Ser(UCN)}$ or mt-$tRNA^{Thr}$ codons on specific transcripts, we performed ribosome profiling to identify codons that are affected by METTL8 levels. Ribosomal complexes from total HEK 293 extracts were separated by sucrose gradient

centrifugation (suppl. Figure 3C). Following MNase digestion, RNA fragments protected by the small mitochondrial ribosomal subunit were cloned and sequenced. This approach allows for the precise mapping of codons in the A, P and E sites of the mitochondrial ribosome. Strikingly, in METTL8 KO cells, codons coding for serine are clearly enriched in the P site suggesting that the dwelling time of ribosomes at serine codons is increased. Threonine codons, however, are not enriched suggesting that C_{32} methylation on the mt-tRNA^{Thr} is not essential for the translation cycle (Figure 7C; similar results were obtained using an independent METTL8 KO clone, suppl. Figure 3D and E). Curiously, under METTL8 overexpression conditions, we did not observe a specific codon enrichment in the P site but in contrast find a clear bias for threonine codons in the A site indicating that the ribosome remain longer on these codons when METTL8 levels are high (Figure 7D). Finally, we asked which specific codons are affected in our analyses (Figure 7E and F). Our bioinformatic analyses revealed that the UCA and UCG/U codons of the mt-tRNA$^{Ser(UCN)}$ appears to be strongly enriched in the P site and UCA in the A site when METTL8 is knocked out (Figure 7E). When METTL8 is overexpressed, the ACC codon of the mt-tRNA^{Thr} is enriched in the A site (Figure 7F). To better define a potential sequence context of the affected codons, we investigated flanking nucleotides (Figure 7G and H). Although overrepresented in our sequencing, we find a mild enrichment of a 5' C for the UCU, UCA and UCG codons in either the P or A site (suppl. Figure 3F and data not shown). However, an A or G downstream of UCA in the P site and an A downstream of UCA in the A site are enriched and thus more severely affected (Figure 7G). A flanking A either up (data not shown) or downstream of the mt-tRNA^{Thr} ACC codon is also enriched in our data. However, this could also be a consequence of sequencing bias (Figure 7H, suppl. Figure 3G and J). Taken together, our data suggest that specific codons of the mt-tRNA substrates of METTL8 are more affected than others, which may lead to changed protein levels and therefore better or worse incorporation into respiratory chain complexes.

Discussion

tRNAs are extensively modified in all kingdoms of life and such chemical alterations affect all aspects of tRNA function including folding, loading with amino acids, binding to the ribosome and recognition and pairing of the anticodon arm with the codon (Suzuki, 2021). Many of these modifications as well as their modifying enzymes have been associated with human diseases including cancer (Bohnsack and Sloan, 2018a; Chujo and Tomizawa, 2021; Delaunay and Frye, 2019; Suzuki, 2021).

The tRNA modification m^3C_{32} on mt-tRNA$^{Ser(UCN)}$ and mt-tRNA^{Thr} has long been known but the responsible enzyme remained elusive (Bohnsack and Sloan, 2018a; Suzuki and Suzuki, 2014). Here we have discovered that METTL8 is a mitochondrial protein that catalyzes C_{32} methylation of these mt-tRNAs. Our biochemical investigations further revealed that METTL8 requires the presence of i^6A on A_{37}, which most likely induces structural rearrangements presenting C_{32} in a configuration that allows METTL8 to access the substrate (Cabello-Villegas et al., 2002; Ganichkin et al., 2011; Murphy et al., 2004; Weixlbaumer et al., 2007). It has been suggested before that METTL8 modifies mRNAs in the cytoplasm and specific R-loop structures in the nucleus (Xu et al., 2017; Zhang et al., 2020). Although our unbiased AlkAniline-Seq experiments do not provide evidence for additional substrates, it cannot be excluded that isoforms lacking the N terminal mitochondrial targeting signal are cell type-specifically expressed, which might target non-mitochondrial RNAs. Interestingly, when we mutated residues in the mitochondrial targeting signal, we observe nucleolar mis-localization and such mis-localization might also be caused by N terminal tagging which might interfere with mitochondrial translocation. Nevertheless, a thorough assessment of METTL8 isoforms will be needed to clarify whether METTL8 has additional functions.

Thirteen genes coding for respiratory chain components and 22 tRNA genes are encoded on the mammalian mitochondrial genome. With the exception of leucine and serine, all amino acids are charged onto a single mt-tRNA. The two serine mt-tRNAs are characterized by specific

structural features but only mt-tRNA$^{Ser(UCN)}$ is methylated at position C_{32} (Anderson et al., 1981; Anderson et al., 1982). Interestingly, our AlkAniline-Seq experiments revealed that only a small portion of this tRNA is C_{32} methylated, at least under the analyzed conditions. Nevertheless, mt-tRNA$^{Ser(UCN)}$ is aminoacylated indicating that the modification is not required for amino acid charging. When METTL8 is knocked out, mt-tRNA$^{Ser(UCN)}$ is not C_{32} methylated at all and our ribosome profiling data revealed that ribosomes tend to dwell longer on UCA and UCG/U codons of mt-tRNA$^{Ser(UCN)}$. Furthermore, the high resolution of our data allowed for mapping the stalled position to the A, P and E site of the mitoribosome. Here we made several interesting observations. First, the cognate codon UCA of the mt-tRNA$^{Ser(UCN)}$ is stalled in the A and the P site (Figure 7E). Closer examination revealed that stalling in the A site is preferentially flanked by a downstream A, while codons stalled in the P site by a downstream G (Figure 7G), which may suggest that a purine downstream of the cognate codon requires m^3C_{32} methylation more than others. Second, specific near-cognate codons are preferentially stalled in the P site independently of the flanking nucleotide. Near-cognate codons engage in wobble pairing at position three of the codon while the cognate codon forms Watson-Crick base pairing between the codon and the anticodon. It is tempting to speculate that m^3C_{32} is important for decoding fully complementary codons when flanked by G, while a flanking A as well as several near-cognate codons require the modification for steps downstream of decoding. This model, however, needs to be further analyzed.

When investigating transcripts that might be important for the observed phenotypes, we find that ND6 has two of the three strongest stalling events, both involving potentially problematic mt-tRNA$^{Ser(UCN)}$ UCU codons, which are also stalled in the P site (Figure 7E and data not shown). At codon 20, ribosomes stall with a UCU codon positioned in both the P and A sites and at position 24 a UCU codon is flanked by proline codons. A reduced ND6 production would also be consistent with our mass spectrometry results, in which ND6 was reproducibly missing

from respiratory chain complexes. This, however, requires deeper and more comprehensive investigations.

METTL8 KO results in a complete loss of C_{32} methylation of mt-tRNA^{Thr}, which appears to be fully methylated within the mitochondrial tRNA pool. Under KO conditions, we did not observe stalled ribosomes suggesting that the methylation is not essential for the translation cycle under tissue culture conditions. Curiously, we identified stalled ribosomes on the ACC mt-tRNA^{Thr} codon when METTL8 is overexpressed. In contrast to mt-tRNA$^{Ser(UCN)}$, ribosomes remain at the A site. By carefully analyzing our Northern blotting experiments (Figure 2C), we observed that mt-tRNA^{Thr} is generally very low abundant. Furthermore, when overexpressing METTL8-F/H we observed further reduction and METTL8 KO revealed stronger mt-tRNA^{Thr} signals (Figure 2C). Thus, METTL8 not only affects the methylation status but also cellular levels of mt-tRNA^{Thr}. Thus, stalled ribosomes at the ACC codon in the A site are consistent with reduced mt-tRNA^{Thr} availability followed by an extended dwelling time of the ribosome at this codon.

Although METTL8 is strongly expressed in a variety of cancers (Figure 5, (Begik et al., 2020)), patient survival is only correlated with high METTL8 levels in pancreatic cancer. Since an increase in METTL8 is accompanied with enhanced respiratory chain activity, an obvious benefit for cancer cells could be a better energy supply allowing fast and aggressive progression (Tataranni et al., 2017). However, given the complexity of the underlying molecular principles, i.e. only a minor portion of mt-tRNA$^{Ser(UCN)}$ is methylated and METTL8 has also effect on mt-tRNA^{Thr} abundance, such a model might be too simplified. An intriguing question that still remains is why only a very specific form of pancreatic cancer uses such an apparent advantage. It is more likely that cell type-specific effects or micro-environmental cues influence METTL8 activity in these cells. It is also possible that glycolysis is increased for the generation of building blocks (Warburg effect) and the generated NADH could in addition to lactate production also be regenerated by an enhanced respiratory chain activity. Although this remains speculation, such a scenario could be supported by our finding that PANC-1 cells show higher

proton leakage compared to control cells (Figure 6C). Nevertheless, METTL8 appears to be a very attractive target for treating the so far incurable pancreas carcinoma. RNA therapeutics, e.g. siRNAs or target mimics could be used for specific inhibition of METTL8 and since such cancer cells appear to be more addicted to METTL8 than other cells, such a treatment could be specific and unproblematic for healthy cells.

Taken together, we provide evidence for a sophisticated balancing system of mitochondrial translation fueled by METTL8-mediated C_{32} methylation of the mt-tRNA$^{Ser(UCN)}$ and mt-tRNA^{Thr} that is important for synthesizing optimal respiratory chain compositions. Although not vital under cell culture conditions, a mis-balancing of this sophisticated gene expression program leads to partially incomplete or functionally compromised respiratory chains.

Limitations of the study

Our work uncovers the enzyme that generates m^3C_{32} on the mitochondrial tRNAs mt-tRNA$^{Ser(UCN)}$ and mt-tRNA^{Thr} and we find that particularly the loss or increase of mt-tRNA$^{Ser(UCN)}$ methylation affects respiratory chain activity. However, we have measured respiratory chain activity in cultured cell lines, which are not in a physiological environment. Many of such cell lines do not rely on oxidative phosphorylation and effects might be different in tissues. Furthermore, we find that mitoribosomes are stalled at codons used by the mt-tRNA$^{Ser(UCN)}$ when the m^3C_{32} is missing. Although we observe effects on the abundance of several mitochondria-encoded proteins in respiratory chain complexes using mass spectrometry, the affected codons are widespread and found on almost all mitochondrial transcripts. We hypothesize that the protein ND6 could be the main affected protein but more work is needed to strengthen this model. Finally, we find that METTL8 is overexpressed in a number of cancers, which has also been observed by others. Based on TCGA and GTex data, overexpression seems to correlate with overall patient survival mainly in pancreatic cancer. An obvious scenario would be that pancreatic cancer cells tune respiratory chain activity via

METTL8 overexpression. However, such an obvious advantage appears to be not selected by other types of cancer and thus it is conceivable that other potentially even indirect effects could be involved. This needs to be further unraveled.

Acknowledgements

We thank S. Ammon, C. Friederich and the mass spectrometry group for excellent support. This work was supported by the Deutsche Forschungsgemeinschaft (DFG) grant SPP 1784/1 and 2, the Bavarian Systems-Biology Network (BioSysNet), Grand Est Region (France) FRCR grant EpiARN and the European Research Council (ERC grant 682291, 'moreRNA'). MM, CAP and CDM were supported by the Medical Research Council core funding (MC_UU_00015/4).

Author contributions

E.S. performed most experiments. J.M. contributed ribosomal profiling data and analysis, V.M., C.A.P and C.D.M. contributed to experiments. R.F. generated monoclonal antibodies, M.R. contributed to respiratory measurements, S.H. contributed to the cancer-associated aspects, P.O., M.M., Y.M., M.H. analyzed data. A.B. and K.D. performed mass spectrometry. E.S., M.H., M.M., M.H. and G.M. designed and discussed experiments. E.S. and G.M. wrote the manuscript.

Declaration of interests

The authors declare no competing interests

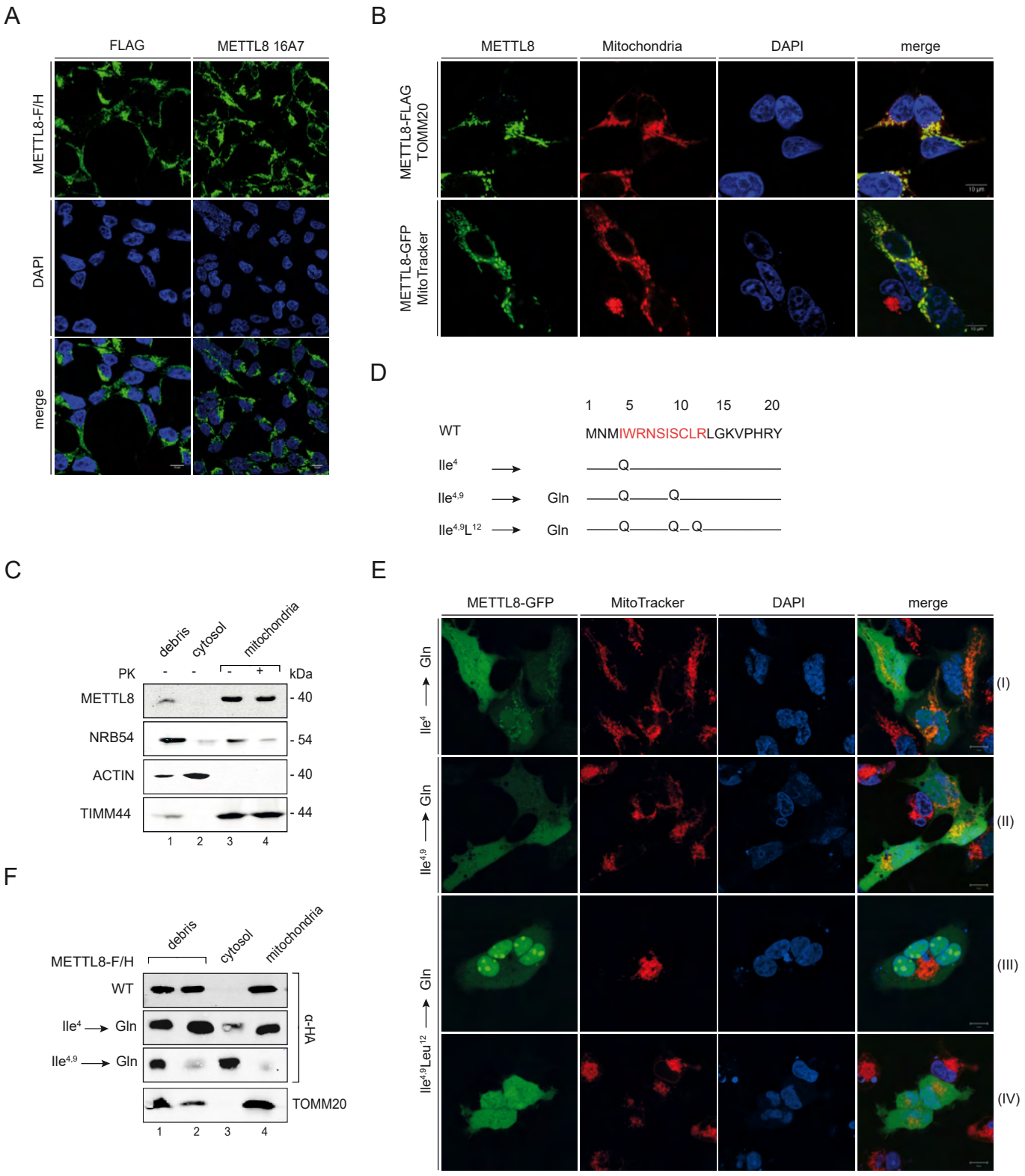
A
FLAG
METTL8 16A7
METTL8-F/H
DAPI
merge
B
METTL8
Mitochondria
DAPI
merge
METTL8-FLAG TOMM20
METTL8-GFP MitoTracker
D
1 5 10 15 20
WT
MNMIWRNSISCLRLGKVPHRY
Ile4 → Q
Ile4,9 → Gln Q Q
Ile4,9L12 → Gln Q Q Q
C
debris
cytosol
mitochondria
PK - - - +
kDa
METTL8 - 40
NRB54 - 54
ACTIN - 40
TIMM44 - 44
1 2 3 4
E
METTL8-GFP
MitoTracker
DAPI
merge
Ile4 → Gln (I)
Ile4,9 → Gln (II)
Gln (III)
Ile4,9Leu12 → Gln (IV)
F
debris
cytosol
mitochondria
METTL8-F/H
WT
Ile4 → Gln
Ile4,9 → Gln
α-HA
TOMM20
1 2 3 4

Figure 1: METTL8 is a mitochondrial localized protein

(A) Immunofluorescence detection of METTL8-F/H by anti-FLAG (green, left panel) and anti-METTL8 16A7 (green, right panel) in Flp-In TREx293 cells. Nuclei were stained with DAPI (blue) (scale bars: 10 µm)

(B) Subcellular localization of METTL8-F/H (green, upper panel) and METTL8-GFP (green, lower panel) in Flp-In TREx293 cells. Top: immunofluorescence detection of METTL8-F/H (green), mitochondrial import receptor subunit TOMM20 (red), and DAPI (blue). Bottom: fluorescence imaging of METTL8-GFP (green), MitoTracker Deep Red (red) and Hoechst 33342 (blue) (scale bars: 10 µm)

(C) Subcellular fractionation of Flp-In TREx293 cells into debris/nuclei (NRB54), cytosol (ACTIN) and mitochondria (TIMM44). Mitochondria were treated with ProteinaseK (PK). Endogenous METTL8 was detectable after anti-METTL8 IP.

(D) Snapshot of predicted MTS pre-sequence with MPP (mitochondrial-processing peptidase) cleavage site (position 20) and mutation of amino acids Ile4,9 and Leu12 to glutamines.

(E) *Live cell imaging* of modified METTL8-GFP (green) by fluorescence detection of MitoTracker Deep Red (red) and Hoechst 33342 (blue). Fluorescence detection of METTL8-GFP single (panel I), double (panel II) and triple MTS mutant (panel III-IV) (scale bars: 10 µm).

(F) Subcellular fractionation of Flp-In TREx293 cells overexpressing METTL8-F/H constructs into debris/nuclei, cytosol and mitochondria. METTL8-F/H was detected by anti-HA, and TOMM20 served as mitochondrial marker.

.

A

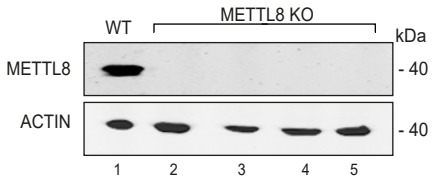
WT
METTL8 KO
kDa
METTL8
- 40
ACTIN
- 40
1 2 3 4 5

B

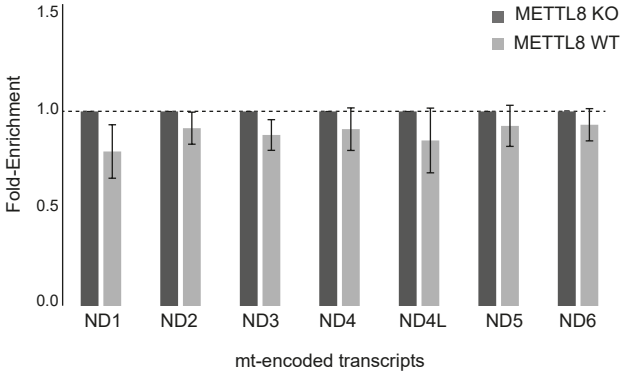
METTL8 KO
METTL8 WT
Fold-Enrichment
1.5
1.0
0.5
0.0
ND1 ND2 ND3 ND4 ND4L ND5 ND6
mt-encoded transcripts

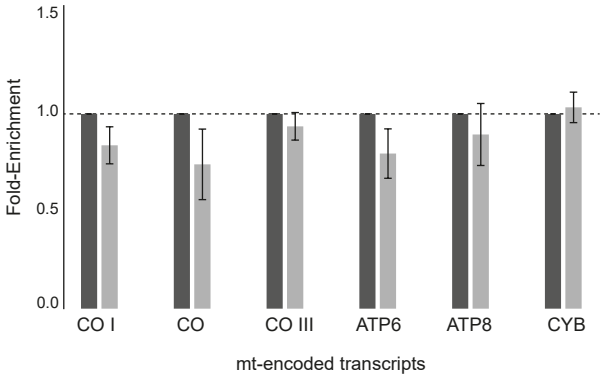
Fold-Enrichment
1.5
1.0
0.5
0.0
CO I CO CO III ATP6 ATP8 CYB
mt-encoded transcripts

C

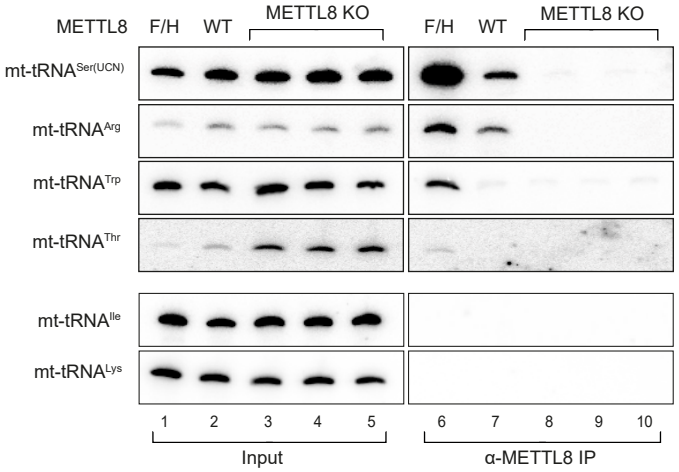
METTL8 F/H WT METTL8 KO F/H WT METTL8 KO
mt-tRNASer(UCN)
mt-tRNAArg
mt-tRNATrp
mt-tRNAThr
mt-tRNAIle
mt-tRNALys
1 2 3 4 5 6 7 8 9 10
Input
α-METTL8 IP

D

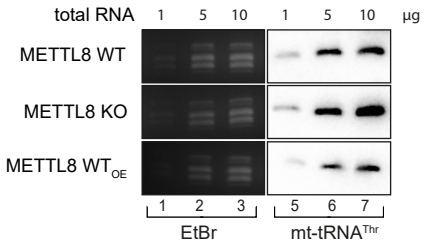
total RNA 1 5 10 1 5 10 µg
METTL8 WT
METTL8 KO
METTL8 WTOE
1 2 3 5 6 7
EtBr
mt-tRNAThr

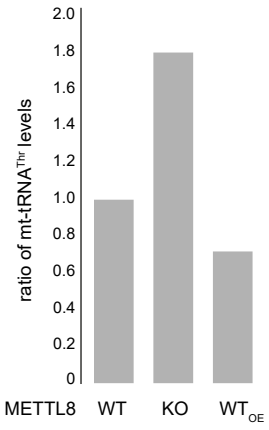
ratio of mt-tRNAThr levels
2.0
1.8
1.6
1.4
1.2
1.0
0.8
0.6
0.4
0.2
0
METTL8 WT KO WTOE

E

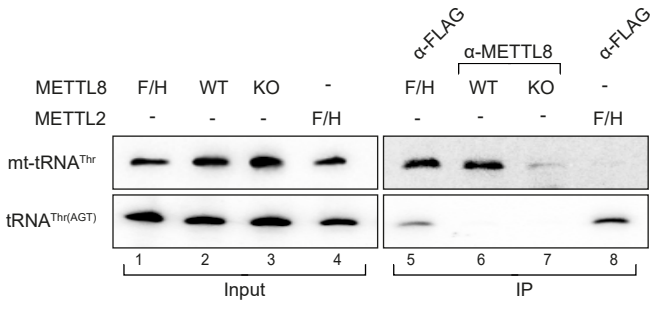
α-FLAG
α-METTL8
α-FLAG
METTL8 F/H WT KO - F/H WT KO -
METTL2 - - - F/H - - - F/H
mt-tRNAThr
tRNAThr(AGT)
1 2 3 4 5 6 7 8
Input
IP

F

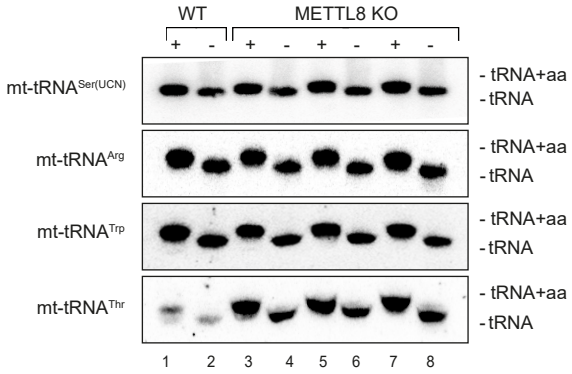
WT
METTL8 KO
+ - + - + - + -
mt-tRNASer(UCN)
mt-tRNAArg
mt-tRNATrp
mt-tRNAThr
- tRNA+aa
- tRNA
1 2 3 4 5 6 7 8

Figure 2: METTL8 interacts with mitochondrial tRNAs

(A) Detection of METTL8 in Flp-In TREx293 METTL8 WT and METTL8 KO cell lines after anti-METTL8 IP. ACTIN served as control.

(B) METTL8 RNA immunoprecipitation (RIP)-qPCR of METTL8 WT and METTL8 KO Flp-In TREx293 cell lines. METTL8 KO cell line was used as control. Mean ± standard error of difference (SED) of three independent measurements are plotted.

(C) Northern Blot analysis of RNA co-immunoprecipitated with METTL8. METTL8 KO cell lines and 0.5 µg total RNA for input were used as controls.

(D) Northern Blot analysis of mt-tRNA^{Thr} levels in overexpressing METTL8 WT, METTL8 WT and KO cell lines. EtBr staining served as loading control. Right panel: corresponding phosphor imaging quantification is shown.

(E) Northern Blot analysis of RNA co-immunoprecipitated with METTL8 and METTL2. METTL8-F/H and F/H-METTL2 were immunoprecipitated by using anti-FLAG. 0.5 µg total RNA was used as input control.

(F) Mitochondrial tRNA aminoacylation (+) and deacylation (-) levels in METTL8 WT and METTL8 KO cell lines.

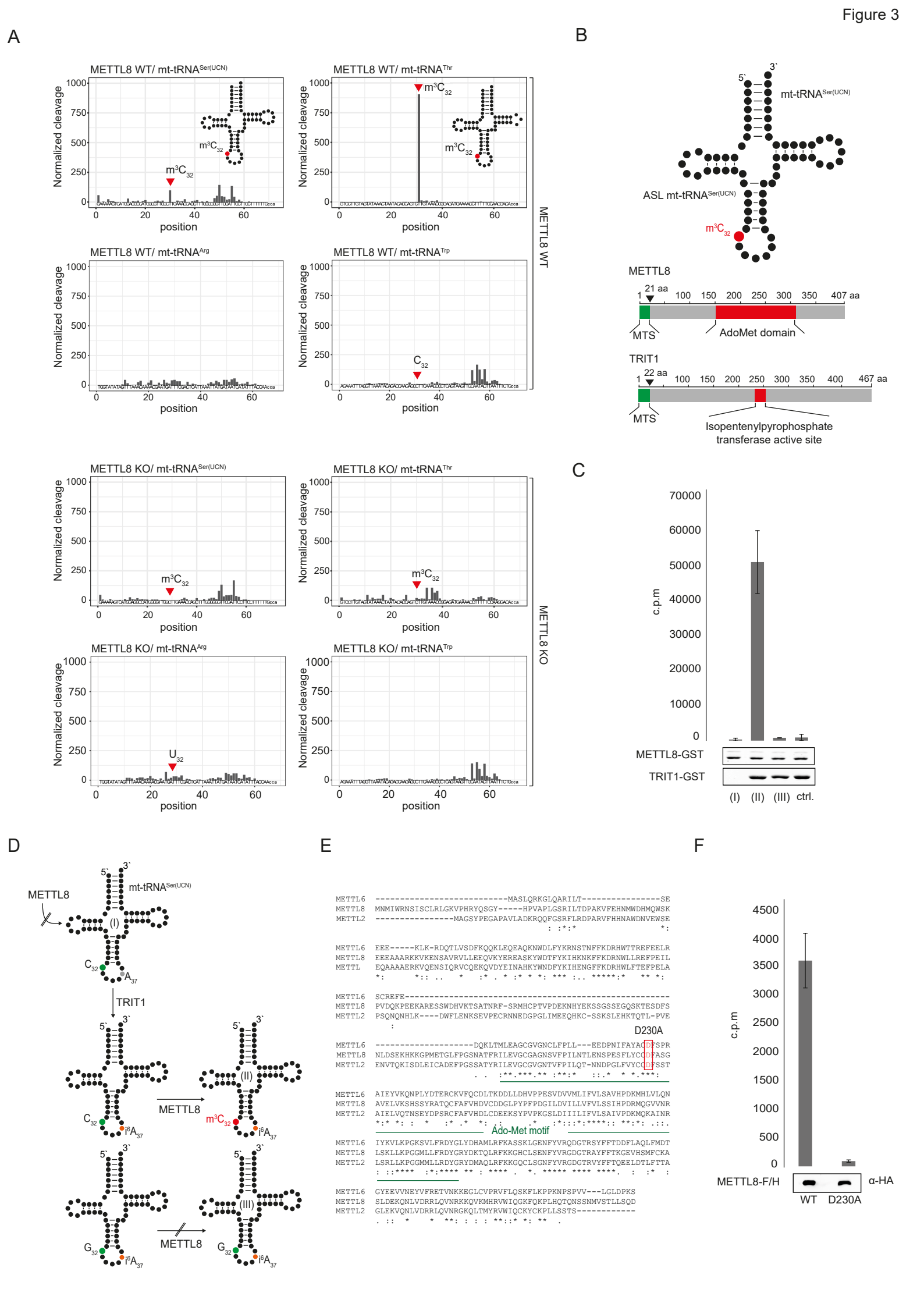
A
METTL8 WT/ mt-tRNASer(UCN)
METTL8 WT/ mt-tRNAThr
METTL8 WT/ mt-tRNAArg
METTL8 WT/ mt-tRNATrp
METTL8 KO/ mt-tRNASer(UCN)
METTL8 KO/ mt-tRNAThr
METTL8 KO/ mt-tRNAArg
METTL8 KO/ mt-tRNATrp
Normalized cleavage
position
m3C32
C32
U32
B
mt-tRNASer(UCN)
ASL mt-tRNASer(UCN)
METTL8
21 aa
407 aa
MTS
AdoMet domain
TRIT1
22 aa
467 aa
Isopentenylpyrophosphate transferase active site
C
c.p.m
METTL8-GST
TRIT1-GST
(I) (II) (III) ctrl.
D
METTL8
TRIT1
mt-tRNASer(UCN)
i6A37
E
D230A
Ado-Met motif
METTL6
METTL8
METTL2
F
c.p.m
METTL8-F/H
α-HA
WT D230A

Figure 3: METTL8 methylates position C_{32} in mt-tRNA$^{Ser(UCN)}$ and mt-tRNA^{Thr}

(A) AlkAniline-Seq analysis of METTL8 WT and METTL8 KO cell lines. Top: m^3C cleavage profiles of mt-tRNA$^{Ser(UCN),}$ mt-tRNA^{Thr}, mt-tRNA^{Arg} and mt-tRNA^{Trp} in METTL8 WT. Bottom: m^3C cleavage profiles in METTL8 KO.

(B) Top: mt-tRNA$^{Ser(UCN)}$ with highlighted anticodon stem loop (ASL). Bottom: cartoon of METTL8 (UniProt: B3KW44) and TRIT1 (Uniprot: Q9H3H1) protein domains. Catalytic domains (S-Adenosyl-Methionine binding site/ Isopentenylpyrophosphate transferase active site) are highlighted in red, mitochondrial targeting signal (MTS) in green.

(C) Methyltransferase activity assay of METTL8-GST. Full length unmodified mt-tRNA$^{Ser(UCN)}$ (column I), i^6A_{37} pre-modified mt-tRNA$^{Ser(UCN)}$ (column II) and i^6A_{37} pre-modified mt-tRNA$^{Ser(UCN)}$ mutant (C32G) (column III) were used as substrates. Mitochondrial i^6A_{37} pre-modified tRNAs Phe, Trp and Ser(AGY) were used as negative controls. Mean ± SED of three to six independent measurements are plotted. As loading control 1 µg recombinant protein was separated on a 10 % SDS gel and stained by Coomassie Blue.

(D) Cartoon of the m^3C formation on mt-tRNA$^{Ser(UCN)}$. Position 32 (green) is methylated (red) after position 37 (black) is isopentenylated (orange).

(E) Multiple sequence alignment of human METTL2B (GenBank: NM_018396.2), METTL6 (GenBank: NM_152396.3) and METTL8 (GenBank: NM_024770.4). Conserved S-Adenosyl-Methionine binding site is highlighted in green. Conserved predicted catalytically residue D230A is highlighted by a red box.

(F) Methylation assay of WT METTL8-F/H and METTL8-F/H D230A variant. Both constructs were enriched by an anti-FLAG IP. Methylation activity was adjusted to western blot signals. I^6A_{37} pre-modified mt-tRNA$^{Ser(UCN)}$ was used as substrate. Mean ± SED of three independent measurements are plotted.

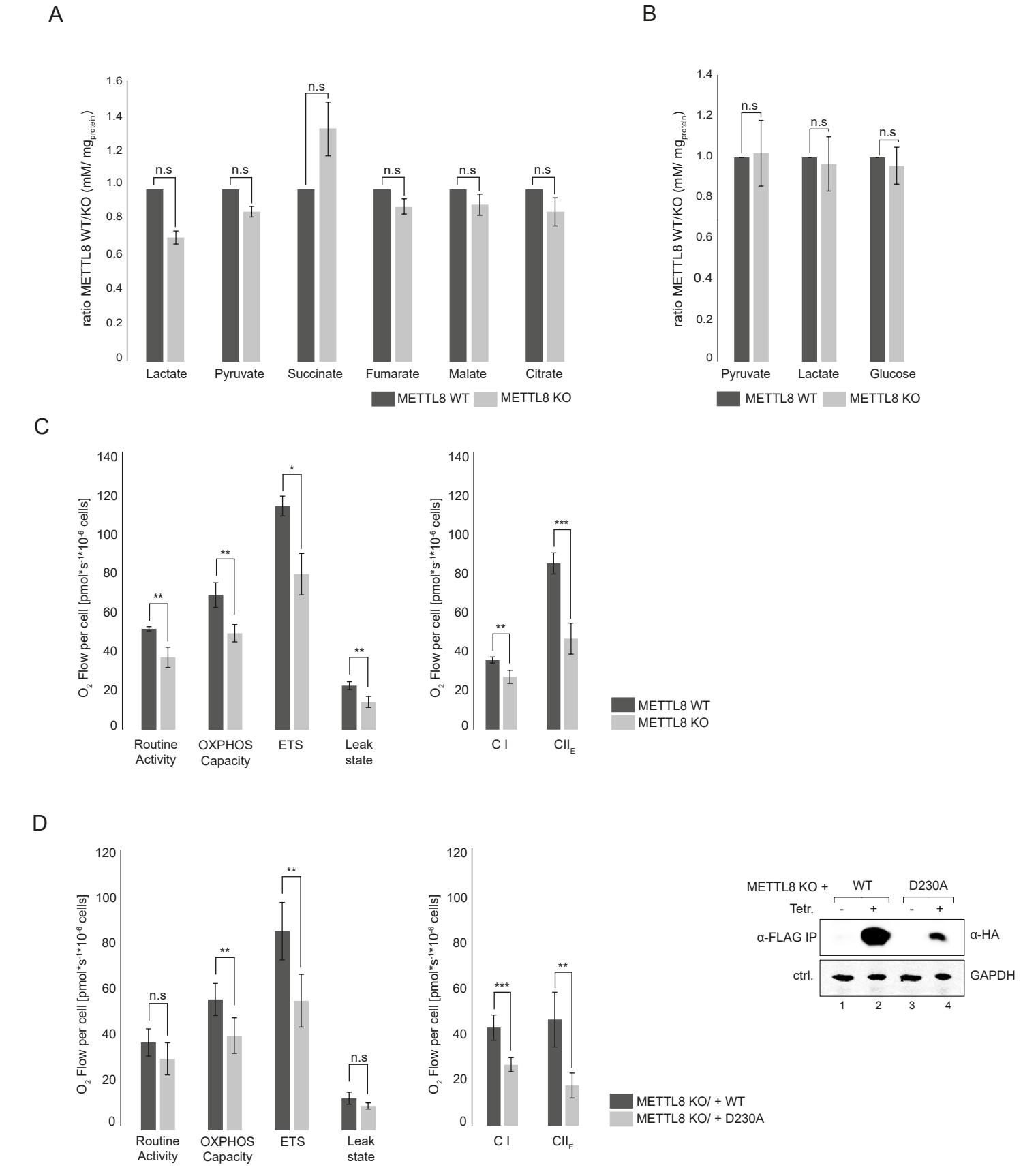
A
ratio METTL8 WT/KO (mM/ mg protein)
n.s
Lactate
Pyruvate
Succinate
Fumarate
Malate
Citrate
METTL8 WT
METTL8 KO
B
ratio METTL8 WT/KO (mM/ mg protein)
n.s
Pyruvate
Lactate
Glucose
METTL8 WT
METTL8 KO
C
O2 Flow per cell [pmol*s-1*10-6 cells]
Routine Activity
OXPHOS Capacity
ETS
Leak state
C I
CIIE
METTL8 WT
METTL8 KO
D
O2 Flow per cell [pmol*s-1*10-6 cells]
Routine Activity
OXPHOS Capacity
ETS
Leak state
C I
CIIE
METTL8 KO/ + WT
METTL8 KO/ + D230A
METTL8 KO +
WT
D230A
Tetr.
α-FLAG IP
α-HA
ctrl.
GAPDH
1 2 3 4

Figure 4: Loss of METTL8 disturbs metabolic balancing and reduces OXPHOS activity

(A) Glycolysis and TCA-cycle intermediates in METTL8 WT (dark grey) and METTL8 KO (light grey) cell lines. Mean values ± SED of three independent measurements are plotted. n.s $p > 0.05$ in *t* test.

(B) Metabolic footprinting of the primary glycolysis carbon sources in METTL8 WT (dark grey) and METTL8 KO (light grey) cell lines. Mean values ± SED of three independent measurements are plotted. n.s $p > 0.05$ in *t* test.

(C) Oxygraph-2k measurements of WT METTL8 (dark grey) and METTL8 KO (light grey) Flp-In-TREx293 cell lines. Respiratory activity analysis was performed using the substrate-uncoupler-inhibitor-titration-protocol (SUIT) with carbonyl caynid 4-(trifluoromethoxy)phenylhydrazone (FCCP). Mean values ± SED of four independent measurements are plotted. * $p < 0.05$, ** $p < 0.01$, *** $p < 0.001$ in *t* test.

(D) Left Oxygraph-2k measurements of Flp-In-TREx293 METTL8 KO rescue variants. Respiratory activity analysis of METTL8 KO_WT-F/H (dark-grey) and METTL8 KO_D230A-F/H (light grey) was performed as described in (C). Mean values ± SED of four independent measurements are plotted. n.s $p > 0.05$, ** $p < 0.01$, *** $p < 0.001$ in *t* test. Right: expression of METTL8 WT-F/H and METTL8 D230A-F/H rescued METTL8 KO Flp-In TREx cell lines after anti-FLAG IP. GAPDH served as control.

Figure 5

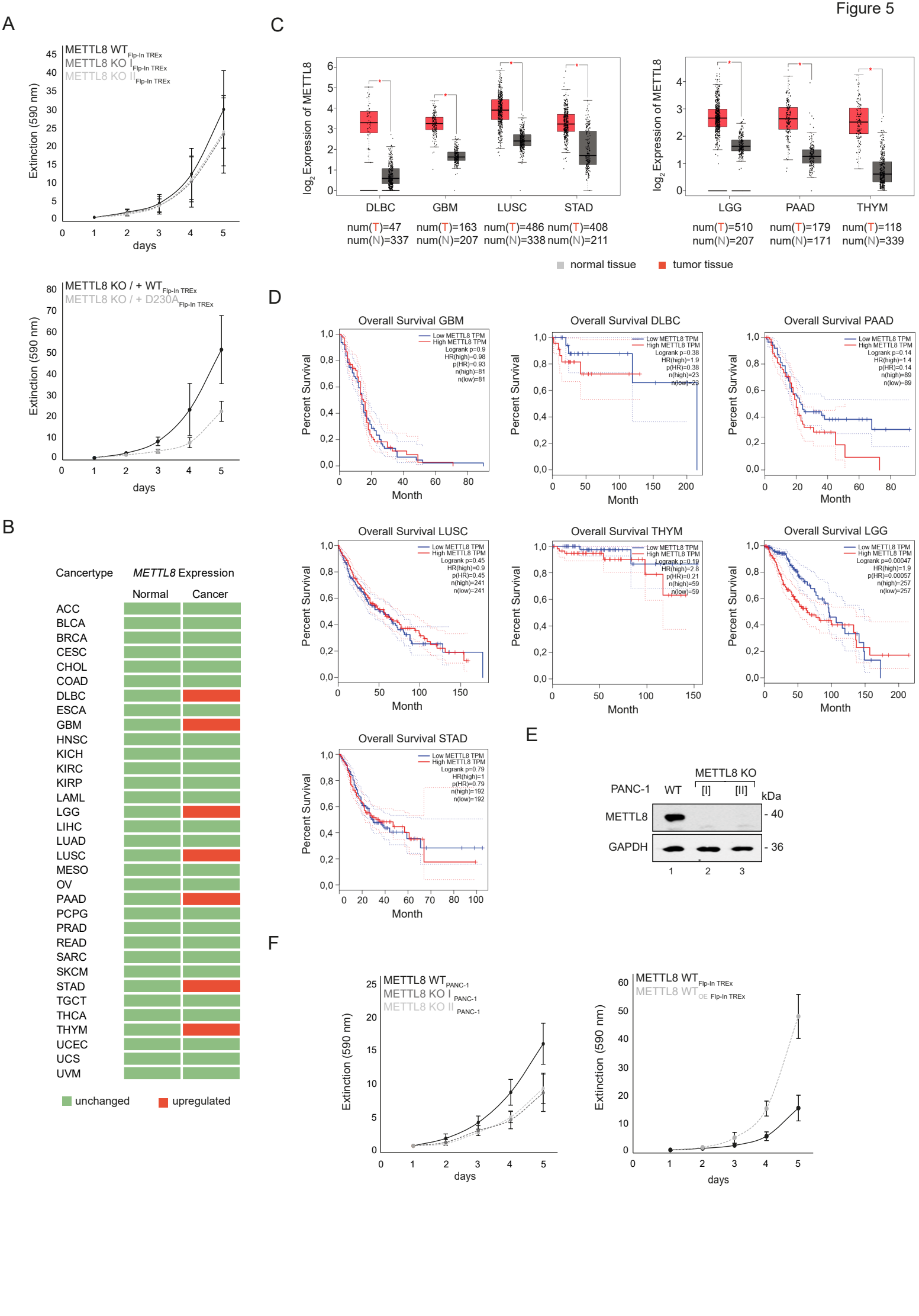
A
METTL8 WT Flp-In TREx
METTL8 KO I Flp-In TREx
METTL8 KO II Flp-In TREx
Extinction (590 nm)
days
METTL8 KO / + WT Flp-In TREx
METTL8 KO / + D230A Flp-In TREx
Extinction (590 nm)
days
B
Cancertype
METTL8 Expression
Normal
Cancer
ACC
BLCA
BRCA
CESC
CHOL
COAD
DLBC
ESCA
GBM
HNSC
KICH
KIRC
KIRP
LAML
LGG
LIHC
LUAD
LUSC
MESO
OV
PAAD
PCPG
PRAD
READ
SARC
SKCM
STAD
TGCT
THCA
THYM
UCEC
UCS
UVM
unchanged
upregulated
C
log2 Expression of METTL8
DLBC
GBM
LUSC
STAD
num(T)=47
num(N)=337
num(T)=163
num(N)=207
num(T)=486
num(N)=338
num(T)=408
num(N)=211
log2 Expression of METTL8
LGG
PAAD
THYM
num(T)=510
num(N)=207
num(T)=179
num(N)=171
num(T)=118
num(N)=339
normal tissue
tumor tissue
D
Overall Survival GBM
Overall Survival DLBC
Overall Survival PAAD
Overall Survival LUSC
Overall Survival THYM
Overall Survival LGG
Overall Survival STAD
Percent Survival
Month
Low METTL8 TPM
High METTL8 TPM
E
PANC-1
WT
METTL8 KO
[I]
[II]
kDa
METTL8
GAPDH
- 40
- 36
1
2
3
F
METTL8 WT PANC-1
METTL8 KO I PANC-1
METTL8 KO II PANC-1
Extinction (590 nm)
days
METTL8 WT Flp-In TREx
METTL8 WT OE Flp-In TREx
Extinction (590 nm)
days

Figure 5: Upregulated METTL8 expression correlates with survival rate in PAAD cancer

(A) The top diagram shows Flp-In TREx293 METTL8 WT cell proliferation in black and METTL8 KO in gray, and the bottom diagram shows growth curves of the Flp-In TREx293 METTL8 KO rescue variants METTL8 KO_WT-F/H (black) and METTL8 KO_D230A-F/H (gray). Cells were grown in presence of high glucose. Mean values ± SED of four independent measurements are plotted.

(B) List of cancer types from GEPIA database (Database: GEPIA). Cancer types with upregulated *METTL8* expression are highlighted in red.

(C) Box plot of METTL8 expression in DLBC, GBM, LGG, LUSC, PAAD, STAD, THYM cancer (red) and normal tissue (grey) based on the GEPIA data set (Database: GEPIA). $p < 0.05$.

(D) Correlation of METTL8 expression and patients overall survival in DLBC, GBM, LGG, LUSC, PAAD, STAD, THYM cancer. Correlation with overall survival with low METTL8 expression (blue) and high METTL8 expression level (red).

(E) Detection of METTL8 in PANC-1 METTL8 WT and METTL8 KO cell lines after anti-METTL8 IP. GAPDH was used as control.

(F) Left: growth curves of PANC-1 METTL8 WT in black and METTL8 KO in gray. Right: proliferation of tetracycline treated METTL8 WT (black) and METTL8 overexpressing (WT_{OE}) (gray) Flp-In TREx293 cells. Cells were grown in presence of high glucose. Mean values ± SED of four independent measurements are plotted.

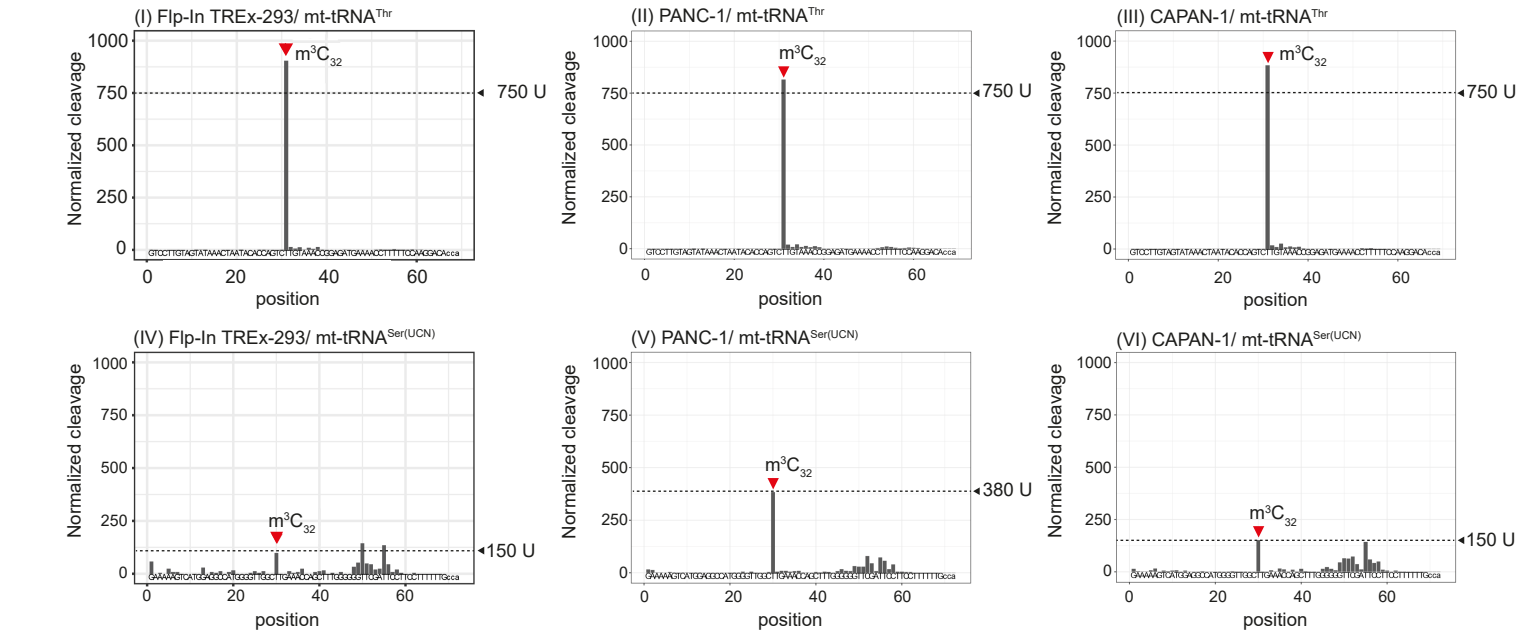
A
(I) Flp-In TREx-293/ mt-tRNA^{Thr}
(II) PANC-1/ mt-tRNA^{Thr}
(III) CAPAN-1/ mt-tRNA^{Thr}
(IV) Flp-In TREx-293/ mt-tRNA$^{Ser(UCN)}$
(V) PANC-1/ mt-tRNA$^{Ser(UCN)}$
(VI) CAPAN-1/ mt-tRNA$^{Ser(UCN)}$
Normalized cleavage
position
m^{3}C$_{32}$
750 U
380 U
150 U

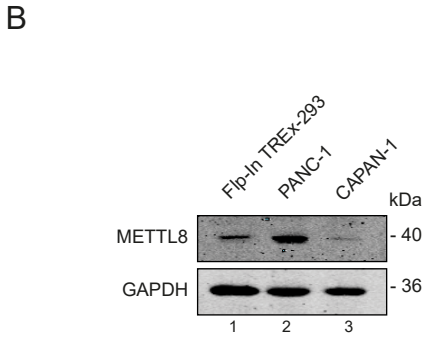
B
Flp-In TREx-293
PANC-1
CAPAN-1
kDa
METTL8
GAPDH
40
36
1
2
3

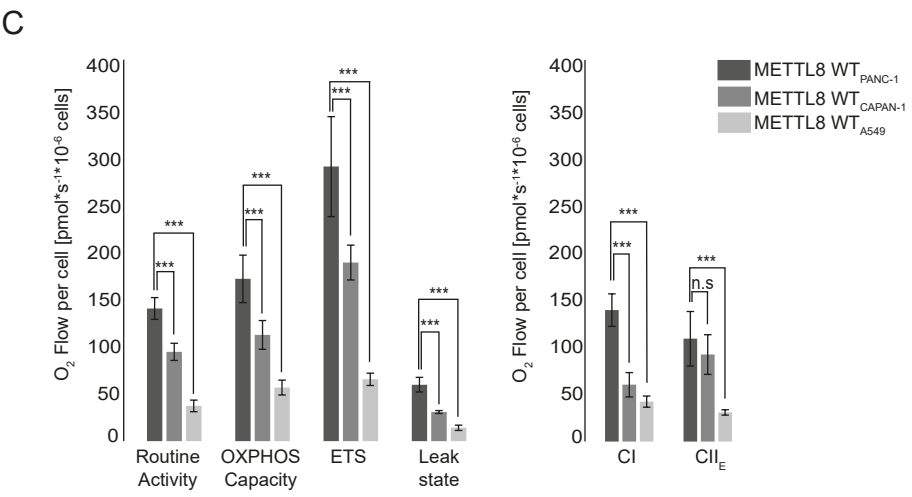
C
O$_2$ Flow per cell [pmol*s^{-1}*10^{-6} cells]
Routine Activity
OXPHOS Capacity
ETS
Leak state
CI
CII$_E$
METTL8 WT$_{PANC-1}$
METTL8 WT$_{CAPAN-1}$
METTL8 WT$_{A549}$
n.s

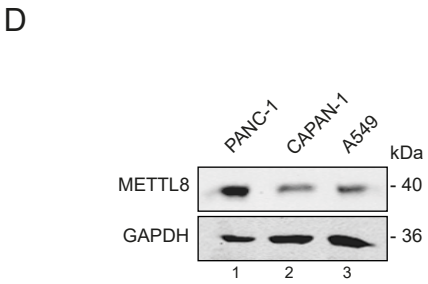
D
PANC-1
CAPAN-1
A549
kDa
METTL8
GAPDH
40
36
1
2
3

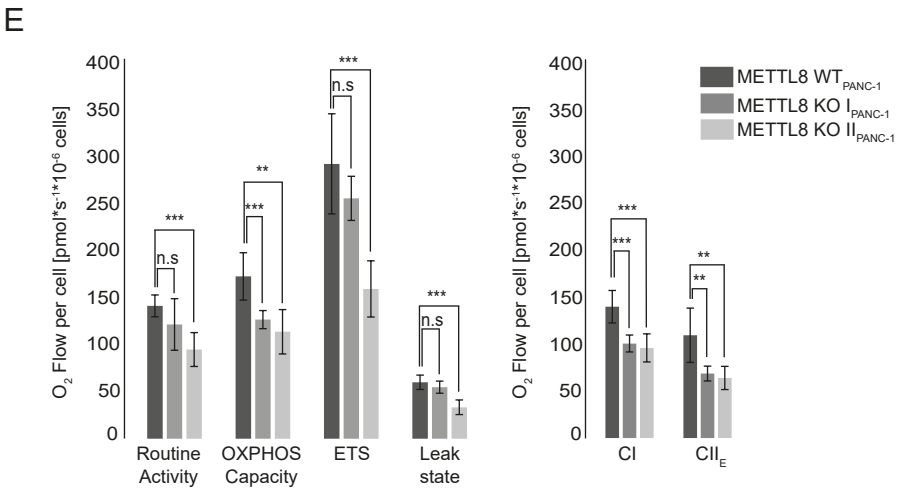
E
O$_2$ Flow per cell [pmol*s^{-1}*10^{-6} cells]
Routine Activity
OXPHOS Capacity
ETS
Leak state
CI
CII$_E$
METTL8 WT$_{PANC-1}$
METTL8 KO I$_{PANC-1}$
METTL8 KO II$_{PANC-1}$
n.s

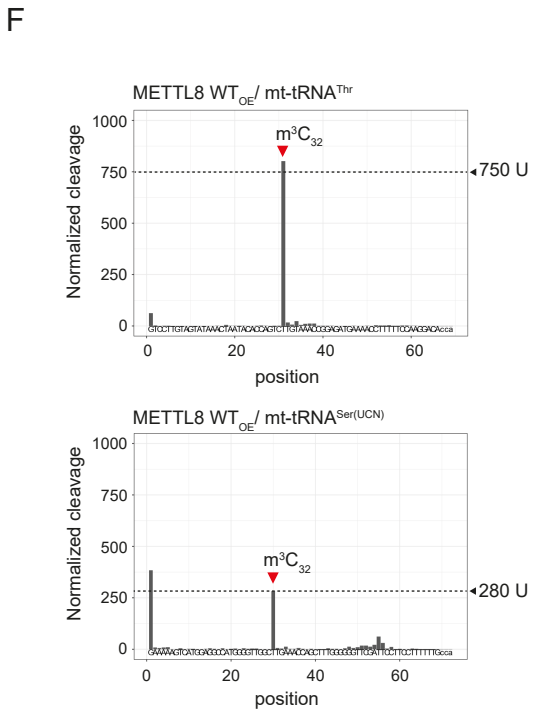
F
METTL8 WT$_{OE}$/ mt-tRNA^{Thr}
METTL8 WT$_{OE}$/ mt-tRNA$^{Ser(UCN)}$
Normalized cleavage
position
m^{3}C$_{32}$
750 U
280 U

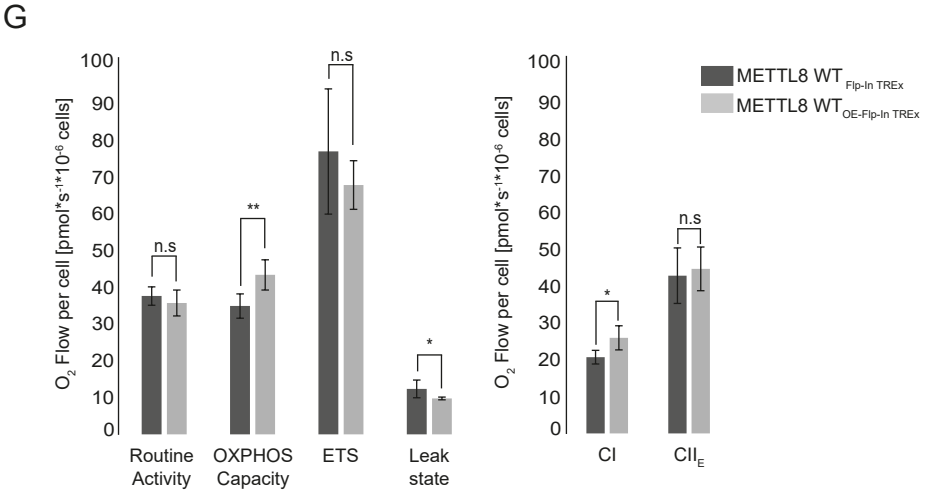
G
O$_2$ Flow per cell [pmol*s^{-1}*10^{-6} cells]
Routine Activity
OXPHOS Capacity
ETS
Leak state
CI
CII$_E$
METTL8 WT$_{Flp-In\ TREx}$
METTL8 WT$_{OE-Flp-In\ TREx}$
n.s

Figure 6: METTL8 expression regulates m^3C_{32} level of mt-tRNA$^{Ser(UCN)}$

(A) AlkAniline-Seq analysis of mt-tRNA^{Thr} and mt-tRNA$^{Ser(UCN)}$ in Flp-In TREx293, PANC-1 and CAPAN-1 cell lines. Top. m^3C cleavage profiles of mt-tRNA^{Thr}. Bottom: m^3C cleavage profiles of mt-tRNA$^{Ser(UCN)}$

(B METTL8 expression level in Flp-In TREx293, PANC-1 and CAPAN-1 cell lines after anti-METTL8 IP. GAPDH was used as control.

(C) Oxygraph-2k measurements of PANC-1 (dark gray), CAPAN-1 (gray) and A549 (light gray) cell line using the SUIT protocol with FCCP. Mean values ± SED of four independent measurements are plotted. n.s $p > 0.05$, ** $p < 0.01$, *** $p < 0.001$ in *t* test.

(D) METTL8 expression level in PANC-1, CAPAN-1 and A549 cell line after anti-METTL8 IP. GAPDH was used as control.

(E) Oxygraph-2k measurements of WT METTL8 (dark gray) and METTL8 KO (light gray) PANC-1 cell lines. Respiratory activity analysis was performed as described in (C). Mean values ± SED of four independent measurements are plotted. n.s $p > 0.05$, ** $p < 0.01$, *** $p < 0.001$ in *t* test.

(F) m^3C cleavage profiles of mt-tRNA^{Thr} (top panel) and mt-tRNA$^{Ser(UCN)}$ (bottom panel) in Flp-In TREx293 cells overexpressing METTL8 WT .

(G) Respiratory activity of METTL8 WT (dark gray) and METTL8 overexpressing (WT_{OE}) (light gray) Flp-In TREx293 cell line analyzed by high-resolution respirometer Oxygraph-2k as described in (C). Mean values ± SED of four independent measurements are plotted. n.s $p > 0.05$, * $p < 0.05$, ** $p < 0.01$ in *t* test

A

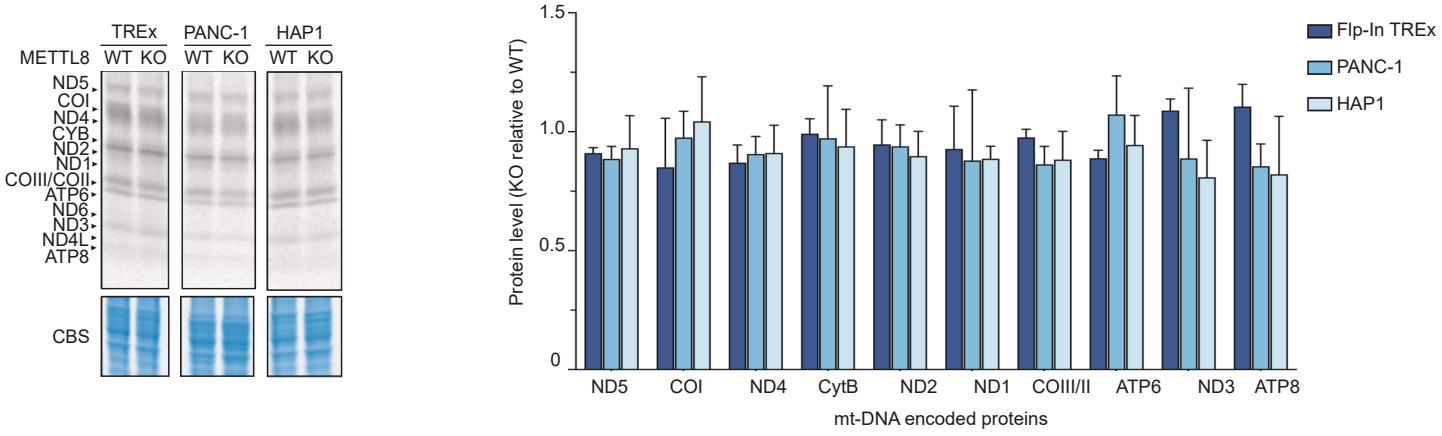

B

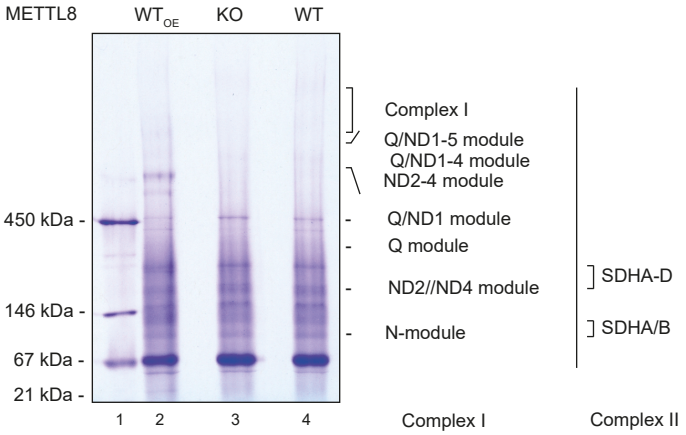

Table 1. Not-detecteable proteins in LC-MS/MS analysis according to their complex submodule

Module	HEK293T WT	METTL8 WT_{OE}	METTL8 KO
N - module	- NDUFS4 - NDUFS6		- NDUFS4 - NDUFS6 - NDUFA6
Q/ND1 module	- NDUFA3		- NDUFA3 - MT-ND1
ND2 module	- NDUFAFA1 - NDUFA1 - NDUFA10		- NDUFAFA1 - NDUFA1 - NDUFA10 - MT-ND6
ND4 module	- NDUFB3 - NDUFAB1		- NDUFB3 - NDUFAB1
ND5 module	- NDUFB5 - NDUFB11		- NDUFB5 - NDUFB11
SDHA-D			- SDHD

C

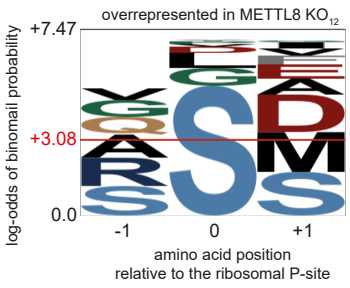

D

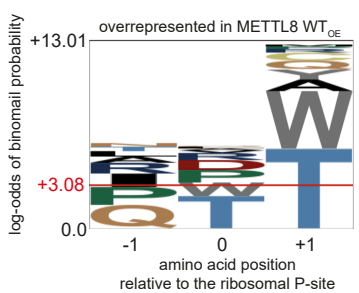

E

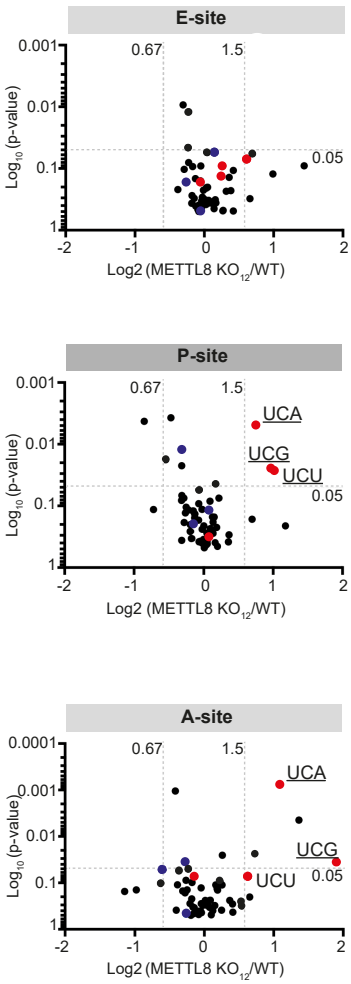

F

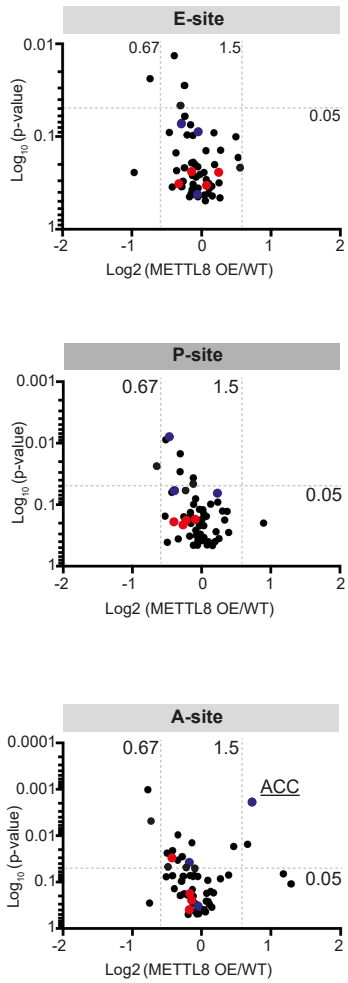

G

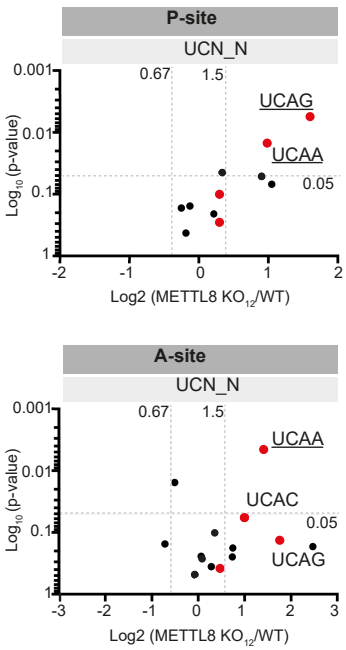

H

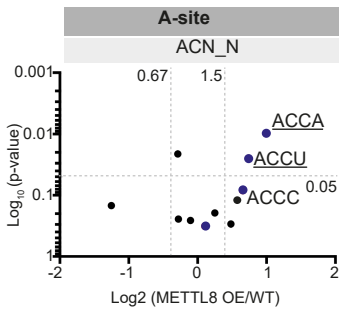

Figure 7: m^3C_{32} unbalancing in mt-tRNA$^{Ser(UCN)}$ and mt-tRNA^{Thr} affects translation dynamics and respiratory complex assembly

(A) Left: radioactive pulse labeling of *de novo* mitochondrial protein synthesis. Flp-In TREx293 and PANC-1 METTL8 WT and METTL8 KO cell lines were labeled with [^{35}S] methionine after cytoplasmic protein synthesis was blocked by emetine dihydrochloride. Total lysates were separated by Tricine-SDS-PAGE and stained with Coomassie Blue as a loading control (left panel). Right: corresponding phosphor imaging quantification. Mean values ± SED of two independent measurements are plotted.

(B) Left: mitochondrial lysates from WT METTL8, METTL8 KO and METTL8 overexpressing (WT_{OE}) Flp-In TREx293 cell lines were separated by blue native (BN) page and analyzed by LC-MS/MS analysis. Assembly of the complex I and II submodules are shown to the side of the panel. Right: listed proteins were not detectable in LC-MS/MS analysis and are mapped to their related module. Additional proteins undetectable in Flp-In TREx METTL8 KO are highlighted in red.

(C) Amino acid overrepresentation at positions relative to the P site in Flp-In TREx293 METTL8 KO cells. Horizontal red line indicates significant overrepresentation.

(D) Amino acid overrepresentation at positions relative to the P site in Flp-In TREx293 cells overexpressing METTL8. Horizontal red line indicates significant overrepresentation.

(E) Ribosomal redistribution in E , P and A site of Flp-In TREx293 METTL8 KO cells based on the codon. Red dots represent mt-tRNA$^{Ser(UCN)}$ codons, mt-tRNA^{Thr} codons are highlighted in blue. Significant overrepresented codons are underlined.

(F) Ribosomal redistribution in E, P and A site of Flp-In TREx293 cells overexpressing METTL8 based on the codon. Red dots represent mt-tRNA$^{Ser(UCN)}$ codons, mt-tRNA^{Thr} codons are highlighted in blue. Significant over- and underrepresented codons are underlined.

(G) Ribosome stalling in either P site or A site of Flp-In TREx293 METTL8 KO cells based on the UCN codon and downstream nucleotides. Left: UCN codons with overrepresented downstream nucleotides in the P site. Right: UCN codons with overrepresented downstream stream nucleotides in the A site. Red dots represent mt-tRNA$^{Ser(UCN)}$ codons. Significantly enriched codons are underlined.

(H) Ribosome stalling in the A site of Flp-In TREx293 cells overexpressing METTL8 based on the ACN codon and downstream nucleotides in the A site. Blue dots represent mt-tRNA^{Thr} codons. Significantly enriched codons are underlined.

STAR METHODS

Lead Contact, Material Availability and Data and Code Availability

Lead contact

Further information and requests for resources and reagents should be directed to and will be fulfilled by the lead contact Gunter Meister (gunter.meister@ur.de).

Materials availability

Plasmids and cell lines generated in this study are shared by the lead contact upon request.

Data and Code availability

MitoRibosome profiling and AlkAnilineSeq data have been deposited at GEO and ENA and are publicly available as of the date of publication. Accession numbers are listed in the key resource table. Original western blot images and microscopy data have been deposited at Mendeley and are publicly available as of the date of publication.

All original code is publicly available as of the date of publication and shared by James Marks (MitoRibosome Profiling) and Yuri Motorin (AlkAnilineSeq) upon request.

Any additional information required to reanalyze the data reported in this paper is available from the lead contact upon request.

EXPERIMENTAL MODEL AND SUBJECT DETAILS

Generation of inducible Flp-In™ T-REx™ -293 cell stable expression cell lines

Inducible Flp-In™ T-REx™ 293 cell lines stably expressing F/H-METTL2B// METTL8-F/H constructs were generated by co-transfection of pcDNA™5/FRT/TO harboring F/H-METTL2B //METTL8-F/H constructs and pOG44 plasmid. Transfection was carried out by Lipofectamin™ 2000 (Invitrogen) reagent according to the manufacture`s protocol. Cells grown in 24-wells were transfected at 80-90 % confluence using 100 ng pcDNA™5/FRT/TO and 900 ng pOG44 plasmid. To select transfectants, cells were cultured in medium supplemented with 15 µg/ml blasticidin and 150 µg/ml hygromycin B.

Generation of METTL8 knockout cell lines

METTL8 knockout (KO) was generated in Flp-In™ T-REx™293 and PANC-1 cell lines by CRISPR/Cas9-directed genome editing. The site-directed frameshift in *METTL8* was guided by the *METTL8* complementary sgRNA (5`-CACCGAGAGAAGCTAGTAAATACT-`3) embedded in a pX459 backbone. Cells were transfected twice by Lipofectamin™ 2000 (Invitrogen) with an intermediary puromycin selection round of 12-16 hours, which was skipped for PANC-1 cells. After transfection and recovering step, cells were separated into single clones. Flp-In™ T-REx™ 293 METTL8 KO clones were analyzed by sequencing strategy and validated by western blotting. For sequencing, genomic DNA of clonal cell lines was extracted by 0.2 mg/ml ProteinaseK (AppliChem) in 500 µl ProteinaseK buffer (200 mM Tris/HCl pH 7.5, 300 mM NaCl, 25 mM EDTA, 2 % [w/v] SDS) at 50 °C overnight. DNA was precipitated by addition of 400 µl 2-propanol and centrifugation at 20 000 g and 4 °C for at least 30 minutes. Pellet was washed twice with 70 % EtOH [v/v], dried 10 minutes at 50 °C and dissolved in 50 µl water. 150 bp region comprising sgRNA annealing site was amplified in a 50 µl PCR reaction (1x Phusion HF Buffer, 200 µM dNTPs, 2x 0.5 µM specific primer, 3 % [v/v] DMSO, 3 µl purified DNA, 1 U Phusion® High-Fidelity DNA Polymerase) (New England BioLabs®). DNA region was amplified by thermocycling and amplicons were purified by a 2 % [w/v] agarose gel, followed by a NucleoSpin Gel and PCR Clean-up Kit (Macherey-Nagel). In a second PCR round, purified amplicons were attached to barcodes of the Illumina TrueSeq-System and sequenced by a MiSeq-sequencing platform. Genotypes of the utilized METTL8 KO cell lines are given below.

METTL8 KO clone	Allele	Genotype
C12_05	1	Insertion 1 nt
	2	Insertion 1 nt
C07_05	1	Deletion 5 nt
	2	Deletion 1 nt

PANC-1 METTL8 KO clones were tested directly by western blotting.

General Cell culture conditions

Cell lines and adherent HeLa S3 were grown in Dulbecco's modified Eagle's medium (DMEM; Sigma Aldrich) supplemented with 10 % fetal bovine serum (FBS; Gibco) under standard conditions at 37 °C in 5 % CO_2 atmosphere. Medium for Flp-In™ T-REx™ 293 cells was completed with 15 µg/ml blasticidin (Gibco) and 100 µg/ml zeocin (Invitrogen), medium for Flp-In™ T-REx™ 293 cell stably expressing METTL2B or METTL8 constructs with 15 µg/ml blasticidin (Gibco) and 150 µg/ml hygromycin B (Invitrogen). HeLa and HAP1 cell lines were treated with antibiotics penicillin (100 U/ml) and streptomycin (100 µg/ml) (Sigma). HeLa S3 suspension cells were expanded in spinner flasks and Joklik`s medium (Sigma Aldrich) supplemented with 10 % fetal bovine serum (FBS; Gibco) at 37 °C.

Name	Species	Tissue	Sex	Disease	Identifier
Flp-In™ T-REx™ 293	human	embryonic kidney	fetus		ATCC® CRL-1573™
PANC-1	human	pancreas/duct	male	epithelioid carcinoma	ATCC® CRL-1649™
CAPAN-1	human	pancreas/derived from metastatic site: liver	male	adenocarcinoma	ATCC® HTB-79™
A549	human	lung	male	carcinoma	ATCC® CCL-185™
HAP1	human		male	chronic myelogenous leukemia	HZGHC005033c009
HeLa	human	cervix	female	adenocarcinoma	ATCC® CCL-2™
HeLa S3	human	cervix	female	adenocarcinoma	ATCC® CCL-2.2™

METHOD DETAILS

Immunofluorescence

HeLa cells for immunofluorescence analysis were grown on coverslips and transiently transfected with METTL8.FLAG.STREP2 using Lipofectamin™ 2000 (Invitrogen) reagent. After 24 h HeLa cells were fixed with 4 % formaldehyde solution and permeabilized with 1 % Triton X-100.

Flp-In™ T-REx™ 293 cells stably expressing METTL8-F/H were grown on coverslips without blasticidin and hygromycinB. Expression was induced by 1 µg/ml tetracycline 24 h before fixation with ice cold acetone at -20 °C for 7 minutes (Alshammari et al., 2016).
Glass slides were incubated in blocking solution (1x TBS, 6 % [w/v] BSA, 0.1 % [v/v] Tween-20) at RT for 1 h, followed by overnight incubation at 4 °C with primary antibody (1x PBS, 3 % [w/v] BSA, 0.1 % [v/v] Tween-20). In the next step glass slides incubated with secondary antibody (1x PBS, 3 % [w/v] BSA, 0.1 % [v/v] Tween-20) at RT for 1 h. Between fixation and antibody treatments five 1x PBS washing steps of 10 minutes were performed. Terminally coverslips were rinsed with water and mounted by using ProLong™ Gold Antifade Mountant with DAPI (Life Technologies). Images were recorded on a Zeiss Axiovert200M microscope and analyzed using Fiji. Used antibodies were listed below.

Primary Antibody	Company	Dilution	Source	Secondary Antibody (Invitrogen)
α-FLAG®M2	Sigma Aldrich (F3165)	1:100-200	mouse, mAb	Alexa Fluor® 488 goat-α-mouse IgG (H+L)
α-TOM20	Santa Cruz Biotechnologies (FL-145)	1:100-200	rabbit, pAb	Alexa Fluor® 555 goat-α-rabbit IgG (H+L)
α-METTL8	Helmholtz Center Munich (MEL8 16A7; 19A10)	1:50-100	rat, mAb	Alexa Fluor® 488 goat-α-rat IgG (H+L)

Live cell Imaging

To analyze the subcellular localization of METTL8-EGFP constructs containing MTS mutations, live cell imaging was performed. Flp-In™ T-REx™ 293 cells were grown in 15 cm dishes and normal DMEM medium on coated coverslips (97 % [v/v] Ham`s F12 Nutrient

Mixture, 1 % [w/v] Fibronectin Solution (Bovine),1 % [w/v] Collagen solution from calf skin, 0.05 % [w/v] BSA, 1 % [v/v] Penicillin-Streptomycin). Cells at 60-70 % confluence were transfected by calcium phosphate (2x HEPES-buffered saline, 2.5 M $CaCl_2$, 10 µg DNA) and grown for additional 48 h under standard conditions. Ahead visualization, cells were washed trice with warm 1x PBS, stained with 1 µg/ml Hoechst 33342 and 133 nM MitoTracker™ Deep Red FM (Invitrogen) in normal growth medium for 20 minutes under standard conditions. Cells were rinsed twice in warm 1x PBS and analyzed on a LSM 710, AxioObserver microscope with a C-Apochromat 63x/1.20 W Korr M27 objective. For detection following filter were used: 450-517 nm (Hoechst 33342), 493-549 nm (EGFP), 638-755 nm (Red FM). Images were analyzed by the software Zen 2011 (Carl Zeiss).

High-resolution Respirometry by Oxygraph-2k

Oxygen consumptions rate was recorded by Oxygraph-2k (O2k; Oroboros Instruments) at 37 °C. Before analysis start, O2k was cleaned and equilibrated with air saturated MIR05 growth medium (20 mM HEPES, 10 mM KH_2PO_4, 20 mM Taurine, 60 mM Lactobionic acid, 3 mM $MgCl_2$, 0.5 mM EGTA, 0.1 % [w/v] BSA) under stirring at 700 rpm. Cells at 70-80 % confluence were washed with warm PBS and detached by Trypsin, which was inactivated after desired incubation time by adding DMEM supplemented with 10 % FBS. Cells were centrifuged at 400 g and RT for 10 minutes, resuspended in MIR05 growth medium and adjusted to a concentration of 0.5x 10^6 cell/ml. For high resolution respirometry analysis 2 ml cell suspension was used and applied to the adapted Substrate-Uncoupler-Inhibitor-Titration Protocol - 001 O2 ce-pce D004 (SUIT; SUIT-001 O2 ce-pce D004). After monitoring routine respiration, plasma membrane was permeabilized by an optimal Digitonin (Merck) concentration depending on cell line.

Cell line	Digitonin [nM]
Flp-In™ T-REx™ 293 METTL8 WT	8.1
Flp-In™ T-REx™ 293 METTL8 KO	8.1
Flp-In™ T-REx™ 293 METTL8 WT_{OE}	8.1
Flp-In™ T-REx™ 293 METTL8 D230A	8.1
PANC-1 METTL8 WT	6.1
PANC-1 METTL8 KO	4.1

LEAK respiration with NADH-linked substrates Glutamate (10 mM; Sigma Aldrich) and Malate (2 mM; Sigma Aldrich) was detected first before stimulating OXPHOS capacity with saturating ADP (5 mM; Calbiochem). Cytochrome *c* (10 µM; Sigma Aldrich) evaluated the integrity of the mitochondrial outer membrane and supported the validity of the respiratory activity. By addition of succinate (10 mM; Sigma Aldrich) the TCA cycle function was reconstituted. After monitoring LEAK respiration in present of ADP by oligomycin (2 mM; Sigma Aldrich), the electron transfer (ET) capacity was stimulated by titration of the uncoupler FCCP (Sigma Aldrich). Rotenone (2 mM; Sigma Aldrich) inhibited complex I and set apart the succinate pathway control state. Terminally complex III was blocked by antimycin (1 mM; Sigma Aldrich) to detect the residual oxygen consumption due to oxidative side reactions.

Proliferation Assay

For proliferation assay 1x 10^3 Flp-In™ T-REx™ 293 cells or 2.5 x 10^3 PANC-1 cells were seeded without any antibiotics in 96-well plates in DMEM without pyruvate and monitored five days under standard conditions. 96-well plates used for Flp-In™ T-REx™ 293 cells were coated with 50 µg/ml Poly-D lysine (Sigma Aldrich) in PBS before. METTL8-F/H expression in Flp-In™ T-REx™ -293 cells was induced by 1 µg/ml tetracycline (AppliChem). After desired incubation time, cells were fixed with 50 µl crystal violet solution (0.5 % [w/v] crystal violet in 20 % [v/v] MeOH) at RT for 10 minutes. Fixed cells were washed twice with 100 µl warm water followed by two further PBS washing steps of two minutes. Lastly cells were rinsed with water and air dried. Cells were quantified by crystal violet intensity detected at 590 nm using a Multimode-Microplate reader Mithras LB 940 (Berthold Technologies). Crystal violet was eluted from the cells before by 50 µl 0.1 M sodium citrate in 50 % [v/v] EtOH.

Plasmids

Open reading frame (ORF) of METTL2B (NM_018396.2), METTL8 (NM_024770.4) and TRIT1 (NM_017646.5) were amplified from Flp-In™ T-REx™ 293 cDNA (SuperScript™ III First-Strand Synthesis System - Invitrogen) using target specific primer with appropriate restriction sites (Table 1) in a 50 µl PCR reaction (1x Phusion HF Buffer, 200 µM dNTPs, 2x 0.5 µM specific primer, 3 % [v/v] DMSO, 0.5 µl cDNA, 1 U Phusion® High-Fidelity DNA Polymerase) (New England BioLabs®). METTL2B amplicon was cloned into a modified pIRES-VP5 backbone encoding a N-terminal FLAG/HA tag using the restrictions enzymes NheI/BglII. METTL8 cDNA was either cloned into a pcDNA5/FRT/TO plasmid encoding

FLAG.STREP2-tag (Minczuk et al., 2011) or into a modified pIRES-VP5 backbone using the restriction enzymes NheI/EcoRI. METTL8 cDNA used for pIRES-VP5 cloning was linked to FLAG/HA tag C- terminally by PCR amplification before cloning into the modified pIRES-VP5 plasmid encoding a N-terminal FLAG/HA tag. Mutations in METTL8 sequence were introduced by site-directed mutagenesis. DpnI digestion at 37 °C for at least 3 h extracted plasmids with incorporated mutation/s. METTL8-EGFP constructs were set up in two consecutive steps. EGFP amplicon, amplified from a random EGFP vector, was imbedded into a modified pIRES-VP5 backbone by using the restriction enzymes NheI/EcoRI. Thereupon METTL8 DNA, amplified from the corresponding VP5 plasmid, were inserted N-terminally by FseI/AscI. For generating tetracycline inducible Flp-In™ T-REx™-293 expression cell lines, METTL8-F/H was inserted into a modified pCDNA™5/FRT/TO vector by AscI/FseI. Recombinant proteins fused to a GST tag at their C-terminus were expressed from a modified pETM14 backbone without a N-terminal 6x His-tag and 3C-site. METTL8 was combined to GST C-terminally by using XbaI/NheI. TRIT1-GST fusion protein was generated by NcoI/NheI. For CRISPR/Cas9-directed genome editing, chimeric guideRNA (sgRNA) complementary to the nearer *METTL8* N-terminus was embedded into the backbone vector pX459. DNA oligonucleotides were phosphorylated in a 10 µl PNK reaction (2x 100 µM DNA oligonucleotide,1x T4 DNA Ligation Buffer, T4 PNK) (Thermo Fisher Scientific) at 37 °C for 30 minutes, boiled up to 95 °C and annealed during cooling down to 25 °C. BbsI digested pX459 backbone and annealed DNA oligonucleotides were ligated at room temperature (RT) for 1 h.

All plasmids and their target sequence were verified by sanger sequencing.

cDNA Synthesis and RNA analysis by Quantitative Real Time RT-PCR

Total volume of RNA isolated from METTL8 immunoprecipitations were reversed transcripted by First-strand cDNA synthesis kit (Thermo Fisher Scientific) using random and mt-tRNA$^{Ser(UCN)}$ specific primer. Fluorometric amplification was performed by Takyon™ No ROX SYBR 2x MasterMix blue dTTP (Eurogentec) with mt-mRNA and mt-tRNASer$^{(UCN)}$ specific primer and CFX96real-Time System (BioRad). Primer sequences are listed in Table 1.

RNA Immunoprecipitation

METTL8-RNA interaction was analyzed by RNA-immunoprecipitation (RIP). Verification of METTL8-RNA interaction was done by either qPCR or Northern Blotting. Flp-In™ T-REx™ 293 METTL8 WT and KO cells were expanded in normal growth medium (DMEM supplemented with 10 % FBS), Flp-In™ T-REx™ 293 cells stably expressing METTL8-F/H were grown overnight in normal growth medium supplemented with 1 µg/ml tetracycline. Cells of 5x 15 cm dishes were harvested and lysed in 1 ml NP-40 lysis buffer (20 mM Tris/HCl pH 8, 137 mM NaCl, 10 % glycerol, 1 % [v/v] NP-40, 2 mM EDTA, 1 mM AEBSF and 1 mM DTT) on ice for 30 minutes. For Northern Blot analysis, living cells were irritated by 280 nm UV light before (120 mJ/cm^2)(Strategene). Cell lysates were cleared at 20 000 g and 4 °C for 30 minutes. Afterwards, samples were adjusted to the same concentration and 10 % of the lysate was used as input sample. For immunoprecipitation 50 µl Protein G Sepharose slurry (GE Healthcare) were used and equilibrated in lysis buffer (20 mM Tris/HCl pH 8, 137 mM NaCl, 10 % glycerol, 1 % [v/v] NP-40, 2 mM EDTA, 1 mM AEBSF and 1 mM DTT). Beads were incubated with 1 ml protein lysate and 5 µg mAb α-METTL8 at 4 °C overnight with rotation. Antibody coupling to protein G was carried out in parallel. FLAG/HA tagged proteins were immunoprecipitated by ANTI-FLAG M2 Affinity Gel (Sigma Aldrich). Next day beads were washed trice with washing buffer (50 mM Tris/HCl pH 8, 300 - 1000 mM NaCl, 0.1 % [v/v] NP-40, 1.5 mM $MgCl_2$, 1 mM AEBSF,1 mM DTT). After transferring beads into a new reaction tube, beads were washed twice again and terminally cleansed in PBS. To isolate the METTL8 bound RNA, proteins were digested first by 6 U/ml ProteinaseK (Thermo Fisher Scientific) in 200 µl ProteinaseK buffer (200 mM Tris/HCl pH 7.5, 300 mM NaCl, 25 mM EDTA, 2 % [w/v] SDS) at 50 °C for 30 minutes while mild shaking. Subsequently RNA was extracted by Roti® Phenol/Chloroform/Isoamylalcohol (Roth) and ethanol precipitation. Total RNA of input samples was purified by TRIzol (Invitrogen).

Northern Blotting including ^{32}P –oligonucleotide labeling

0.5 µg total RNA and RNA derived from METTL8 IP were separated on a 6 % urea-PAGE running at 400 V in 1x TBE buffer. After electrophoresis, RNA quality was checked by EtBr staining first and transferred onto a water equilibrated Hybond™ -N membrane (GE Healthcare) at 20 V for 45 minutes by semi dry blotting (SD Semi-Dry Transfer Cell, Bio-RAD). EDC (1-ethyl-3-(3-dimethylaminopropyl) - carbodiimide hydrochloride) (160 mM EDC, 130 mM 1-methylimidazol, adjusted to pH 8 by HCl) crosslinked RNA to the membrane

at 50 °C in 1 h. Crosslink was completed with UV light at 254 nm (120 mJ/cm^2) (Stratagene). Membrane was rinsed with water and air dried. Meanwhile 20 pmol of DNA oligonucleotide (Table 1) were 5` end labeled by using 0.5 U/ml Polynucleotide Kinase (PNK)(Thermo Fisher Scientific) and 20 mC$_i$ γ-^{32}P-ATP (Hartmann Analytic). PNK reaction was carried out in PNK Buffer A (Thermo Fisher Scientific) 30 minutes at 37 °C and stopped by addition of 18 mM EDTA. [^{32}P] radiolabelled DNA was purified by illustra^{TM} MicroSpin G-25 column (GE Healthcare) and mixed with hybridization solution (20 mM sodium phosphate buffer pH 7.2, 5x SSC, 1 % [w/v] SDS, 2 % [v/v] Denhardt's solution). Hybridization between RNA and radioactive labelled DNA was carrying out overnight at 50 °C. After 12-15 h membrane was washed twice with washing solution I (5x SSC, 1 % [w/v] SDS) and once with washing solution II (1x SSC, 1 % [w/v] SDS) at 50 °C for 10 minutes. Radioactive signals were detected by storage phosphor screens and Personal Molecular Imager^{TM} System (BioRad) with Quantity One Software (version 4.6.9, Bio-Rad). Membrane was interrogated several times with different probes by consecutive stripping and re-probing. For stripping, membrane was washed twice in hot 0.1 % [w/v] SDS solution for 10 minutes with agitation and cleaned with hot water for another 10 minutes.

Aminoacylation Assay

RNA for aminoacylation assay was extracted by TRIzol (Invitrogen). To keep charged tRNAs, all steps were performed on ice and RNA was treated under acid conditions. Aminoacylated RNA was dissolved in 10 mM NaOAc/ HOAc (pH 4.8) at 37 °C for 5 minutes. Deacylated RNA was resuspended in 0.2 M Tris/HCl pH 9.5 and dissolved 1 h at 37 °C. 10 µg of either charged or uncharged RNA was mixed with acid denaturing sample buffer (90 % [v/v] formamide, 0.1 M NaOAc/ HOAc (pH 4.8), 0.05 % [w/v] bromophenol blue and 0.05 % [w/v] xylene cyanol) and separated on a 6 % urea-PAGE containing 0.1 M NaOAc/ OHAc (pH 4.8). Electrophoresis was running at 100 V and 4 °C in 0.1 M NaOAc/ OHAc (pH 4.8) overnight. Separated RNA was transferred onto a water equilibrated Hybond^{TM} -N membrane (GE Healthcare) at 20 V for 30 minutes by semi dry blotting (SD Semi-Dry Transfer Cell, Bio-RAD). RNA crosslinking and visualization were performed according to Northern blotting.

AlkAnilineSeq

Analysis of m^3C residues in human cytoplasmic and mitochondrial tRNAs was performed as described previously (Marchand et al., 2018). In brief, total RNA sample was subjected to partial alkaline hydrolysis in bicarbonate buffer (96 °C, pH 9.2), the reaction was stopped by ethanol precipitation. RNA fragments were extensively de-phosphorylated by Antarctic phosphatase and subjected to aniline cleavage (1M pH 4.5, 15 min in the dark). Resulting fragments having a 5'-phosphate at N+1 nucleotide were converted to a sequencing library using NEBNext Small RNA kit. Sequencing was performed in single-read 50 nt (SR50) mode on HiSeq1000 (Illumina). Sequencing reads were trimmed to remove adapter sequence and aligned to human tRNA reference sequence (both cytoplasmic and mitochondrial tRNAs). Normalized cleavage is calculated as a 1000x ratio of reads starting at a given position to total number of sequencing reads mapped to a given RNA. Please notice that the calibration curve for modification rate to Normalized cleavage is non-linear and shows very high sensitivity for very low modification rates.

Primer Extension Analysis of m^3C_{32}.

Total RNA from WT and METTL8 KO cells was isolated using TRIzol (ThermoFisher) according to the manufacturer's instructions. The subsequent primer extension assay was performed essentially as previously (Rorbach et al., 2014), with the exception that dTTP was excluded from the reaction in order to cause primer stalling downstream of C_{32}. The following primers were used:

Primer	
m^3C_{32}_mt-$tRNA^{Ser(UCN)}$	5' aatcgaacccccaaagctggtttc 3'
m^3C_{32}_mt-$tRNA^{Thr}$	5` aaaaaggttttcatctccggtttac`3

***In vitro* Transcription of mt-tRNAs**

tRNAs were transcribed by T7 RNA polymerase. 100 µM 5` and 3` DNA oligonucleotides linked to T7 promotor sequence (Table 1) (Metabion) were boiled up at 95 °C for 30 seconds in 1x T4 DNA Ligation Buffer (Thermo Fisher Scientific) and annealed by cooling down to 25 °C. Annealed DNA oligonucleotides were transcribed in a 1 ml transcription reaction (30 mM

Tris pH 8.0, 10 mM DTT, 0.01 % [v/v] Triton X-100, 25 mM $MgCl_2$, 2 mM spermidine, 30 % [v/v] DMSO, 5 mM ADP, 5 mM CTP, 5 mM UTP, 5 mM GTP, 0.4 U/ml thermostable inorganic pyrophosphatase (NEB) and 0.1 mg/ml T7-polymerase) overnight at 37 °C. After 12-14 h transcription reaction was mixed with 2x RNA denaturing sample buffer and purified by a 6 % urea-PAGE. RNA was visualized by UV shadowing, cut out and extracted by RNA elution buffer (300 mM NaCl, 2 mM EDTA) overnight with agitation at 4 °C. By adding 0.7 volume 2-propanol RNA precipitated at -20 °C overnight. RNA was pelleted at 20 000 g and 4 °C for at least 30 minutes, washed twice with 80 % [v/v] ethanol, dried at 37 °C for 5 minutes and dissolved in water at 65 °C for 5 minutes.

In vitro m^3C design on mt-$tRNA^{Ser(UCN)}$ (Isopentenylation// Methylation Assay)

m^3C incorporation on mt-$tRNA^{Ser(UCN)}$ catalyzed by METTL8 depends on an isopentenylation reaction at A_{37} (i^6A_{37}). N^6-isopentenyladenosine was introduce in 1 µM mt-tRNA by 250 nM TRIT1 and 10 µM γ,γ-Dimethylallyl pyrophosphate (DMAPP)(Sigma Aldrich). Reaction was carried out in isopentenylation buffer (50 mM Tris/HCl pH 7.5, 5 mM $MgCl_2$, 100 µM β-mercaptoethanol, 0.2 U/ml RiboLock RNase Inhibitor (Thermo Fisher Scientific)) at 37 °C for 1 h (Lamichhane et al., 2013). Modified RNA was isolated by TRIzol extraction (Invitrogen) according to the manufacture`s protocol. RNA pellet was resuspended in 10 µl water and used for the consecutive methylation assay. m^3C incorporation was performed by 250 nM METTL8 in methylation buffer (10 mM Tris/HCl pH 7.5, 100 mM KCl, 1.8 mM $MgCl_2$, 5 % [v/v] Glycerol, 0.1 mg/ml BSA, 1 mM DTT, 0.2 U/mL RiboLock RNase Inhibitor (Thermo Fisher Scientific), 10 nC_i/µl SAM[^{3}H] (Hartmann Analytic)) at 37 °C for 1 h. m^3C modified tRNA was purified by TRIzol extraction (Invitrogen) according to the manufacture`s protocol and resuspended in 25 µl water (65 °C for 5 minutes). RNA was mixed with 10 ml scintillations cocktail (Zinsser Analytic) and measured by a multipurpose scintillation counter (Beckmann Coulter LS6500). Activity was counted per minute (c.p.m.).

Generation of monoclonal Antibodies

A peptide comprising amino acids $_{149}$VPDEKNHYEKSSG$_{161}$ from human METTL8 protein was synthesized and coupled to ovalbumin (Peps4LS, Heidelberg, Germany). Lou/c rats were immunized subcutaneously and intraperitoneally with a mixture of 50 µg OVA-peptide, 5 nmol CPG oligonucleotide (Tib Molbiol, Berlin), 500 µl PBS and 500 µl Incomplete Freund's

adjuvant (IFA). Eight week later, a boost injection without IFA was given three days before fusion of rat spleen cells with P3X63Ag8.653 myeloma cells using standard procedures. Hybridoma supernatants were screened by ELISA for binding to biotinylated METTL8 peptide on avidin-coated ELISA plates. Positive supernatants were further validated in immunoprecipitations and Western blot analysis. Hybridoma cells from selected supernatants were subcloned twice by limiting dilution to obtain stable monoclonal cell lines. Experiments in this work were performed with supernatants from monoclonal antibody clones MEL8 19A10 and 16A7(both rat IgG2c/k).

Cell lysis – Immunoprecipitation – Western Blotting

Cells for immunoprecipitation (IP) were generally broken up by 1 ml NP-40 lysis buffer (20 mM Tris/HCl pH 8, 137 mM NaCl, 10 % glycerol, 1 % [v/v] NP-40, 2 mM EDTA, 1 mM AEBSF and 1 mM DTT). PANC-1, CAPAN-1 and A459 cells were disrupted by glass beads additionally. Cells were lysed 30 minutes on ice and centrifuged at 20 000 g at 4 °C for 30 minutes.

Lysates were adjusted to the same protein concentration by Bradford assay. For immunoprecipitation 50 µl Protein G Sepharose slurry (GE Healthcare) was used and equilibrated in NP-40 lysis buffer. Protein lysates adjusted to the same protein concentration by Bradford were incubated with equilibrated Protein G Sepharose and 5 µg mAb α-METTL8 at 4 °C overnight with agitation. 10 % of the protein lysate was used as input control. F/H tagged proteins were immunoprecipitated by ANTI-FLAG M2 Affinity Gel (Sigma Aldrich). In the next step beads were washed trice with washing buffer (50 mM Tris/HCl pH 8, 300 mM NaCl, 0.1 % [v/v] NP-40, 1.5 mM $MgCl_2$, 1 mM AEBSF,1 mM DTT). After the third washing step beads were transferred into a new reaction tube and washed twice again. Immunoprecipitated proteins were eluted by 5x SDS loading buffer. Input samples were mixed with 1x SDS loading buffer. Samples were boiled at 95 °C for 5 minutes and separated by a 10 % SDS-PAGE. Proteins were transferred onto a nitrocellulose membrane (0.45 µm, GE Healthcare) by semi dry blotting (SD Semi-Dry Transfer Cell, Bio-RAD). Nitrocellulose membrane was blocked in 5 % [w/v] milk at RT for 15-60 minutes and subsequently incubated with primary antibody overnight at 4 °C with agitation. Secondary antibody was applied afterwards for 1 h at RT. Between and after antibody application membrane was washed 3x with 1x TBST for 10 minutes with agitation. Used antibodies were listed below. Signals were detected by Odyssey Infrared

Imaging System (LI-COR Biosciences). Gels for LC-MS/MS analysis were stained by Coomassie Blue (0.25 % [w/v] Coomassie Brilliant Blue R250 (#1610400, Bio-Rad),10 % [v/v] acetic acid, 30 % [v/v] ethanol) and cleansed afterwards with destainer (10 % [v/v] acetic acid, 30 % [v/v] ethanol).

Primary Antibody	Company	Dilution 5 % [w/v]	Source	Incubation	Secondary Antibody (LI-COR)
α-HA.11	Covance (clone 16B12)	1:1000 / milk	mouse, mAb	o/n // 4 °C	IRDye® 800CW Goat α-mouse IgG
α- β Actin	Abcam (ab6276)	1:10000 / milk	mouse, mAb	o/n // 4 °C	IRDye® 800CW Goat α-mouse IgG
α-METTL8	Helmholtz Center Munich (MEL8 16A7; 19A10)	1:500 / milk	rat, mAb	o/n // 4 °C	IRDye® 800CW Goat α-rat IgG
α-TIMM44	ProteinTech	1:3000 / milk	rabbit, pAb	o/n // 4 °C	IRDye® 800CW Goat α-rabbit IgG
α-GAPDH	GeneTEx (GT239)	1:1000 / milk	mouse, mAb	o/n // 4 °C	IRDye® 800CW Goat α-mouse IgG
α- p54[nrb]	BD Transduction Laboratories	1:1000 / milk	mouse, mAb	o/n // 4 °C	IRDye® 800CW Goat α-mouse IgG

Protein expression and purification

METTL8 (aa. 22-407) and TRIT1 (aa. 23-467) were expressed as GST-fusion protein from pETM-14 vector in *E.coli* Rosetta without mitochondrial targeting sequence (MTS). Bacteria were grown to an OD_{600} of 0.5 and cool down at 4 °C until OD_{600} of 0.6. Protein expression was subsequently induced by 100 µM IPTG. TRIT1-GST was expressed 6 hours at 37 °C, METTL8-GST overnight at 23 °C. Bacteria pellet was resuspended in lysis buffer (20 mM Tris/HCl pH 8, 1 M NaCl, 0.2 mM EDTA, 1 mM DTT) and sonicated 3x 5 minutes (duty cycle 50 %, output control 5) with a consecutive break of 5 minutes on ice. Lysate was cleared by centrifugation at 50 000 g and 4 °C for 45 minutes. Before performing GST-pulldown by using a 6 ml GST-column (GE Healthcare), supernatant was passed through a filter with a diameter of 45 µm (Roth). To remove proteins bound unspecifically, column was washed industriously

with lysis buffer and protein of interest was finally eluted with 50 mM Tris/HCl pH 8 and 10 mM Glutathion. The eluate was concentrated to a volume of 0.5-1 ml by Vivaspin® 20 ultrafiltration device (MWCO 30 000, Sartorius) and loaded on a Superdex™ 200 10/30 GL (GE Healthcare) equilibrated with 25 mM Tris/HCl pH 8 and 150 mM NaCl. Peak fractions were analyzed by a 10 % SDS-PAGE, pooled, adjusted to 50 % [v/v] glycerol and stored at -80 °C.

Mitochondrial Preparation

Flp-In™ T-REx™-293 cells from a confluent 15 cm dish were resuspended in 1 ml trehalose buffer (10 mM HEPES/KO pH 6.9, 10 mM KCl, 300 mM trehalose, 0.1 % [w/v] BSA, 0.2 % [w/v] Digitonin) and gently disrupted by using a Potter S Homogenizer (B. Braun Biotech International – sartorius group). Up down movement of the PTFE plungers at 700 rpm ruptured the cell membrane, which was subsequently pelletized at 800 g for 7 minutes at 4 °C. In this centrifugation step nuclei were sediment as well. To separate mitochondria from the cytosol, supernatant was centrifuged at 10 000 g and 4 °C for 10 minutes. Mitochondria were washed trice with trehalose buffer and pelletized at 10 000 g and 4 °C for 5 minutes. To reduce contaminants, mitochondria were resuspended in 1 ml trehalose buffer containing 3 µU/ml ProteinaseK (Thermo Fisher Scientific) and incubated 20 minutes on ice. The reaction was stopped by 2 µg/ ml Aprotinin (Roche), 1 mM AEBSF and centrifugation (10 000 g at 4 °C, 5 minutes). After two washing steps with trehalose buffer, mitochondria were used in BN experiments.

Blue Native Gel Electrophoresis (BN)

120 µg mitochondria were resuspended in 100 µl non-denaturing buffer (20 mM Tris/HCl pH 8, 1 mM sucrose, 1 %, [w/v] Digitonin) and solubilized 30 minutes on ice. Insoluble proteins were pelletized at 20 000 g and 4 °C for 30 minutes. Native protein migration was performed by using SERVA*Gel*™ Native Gel Starter Kit. Solubilized mitochondrial proteins were mixed with 2x Sample buffer for BN and separated on a SERVA*Gel*™ N 3-12 (vertical native gel 3-12 %). Electrophoresis was running 120 minutes at 50-200 V in anode and blue cathode buffer. Blue cathode buffer was exchanged after 2/3 of the electrophoresis. For LC-MS/MS analysis, proteins were fixed in 20 % [w/v] trichloroacetic acid at RT for 30 minutes and stained with Coomassie blue (0.1 % [w/v] Coomassie Brilliant Blue R250 (# 1610400, Bio-Rad), 10 % [v/v]

acetic acid, 45 % [v/v] ethanol). After 30 minutes, gel was cleansed 2x 60 minutes with destainer (20 % [v/v] ethanol, 5 % [v/v] acetic acid, 1 % [w/v] glycerol) and prepared for LC-MS/MS analysis.

Protein Analysis by Mass Spectrometry

For mass spectrometric analysis of proteins gel lanes were cut into consecutive slices. The gel slices were then transferred into 2ml micro tubes (Eppendorf) and washed with 50 mM NH_4HCO_3, 50mM NH_4HCO_3/acetonitrile (3/1) and 50mM NH_4HCO_3/acetonitrile (1/1) while shaking gently in an orbital shaker (VXR basic Vibrax, IKA). Gel pieces were lyophilized after shrinking by 100% acetonitrile. To block cysteines, reduction with DTT was carried out for 30 min at 57°C followed by an alkylation step with iodoacetamide for 30 min at room temperature in the dark. Subsequently, gel slices were washed and lyophilized again as described above. Proteins were subjected to *in gel* tryptic digest overnight at 37°C with approximately 2 µg trypsin per 100 µl gel volume (Trypsin Gold, mass spectrometry grade, Promega). Peptides were eluted twice with 100 mM NH_4HCO_3 followed by an additional extraction with 50 mM NH_4HCO_3 in 50% acetonitrile. Prior to LC-MS/MS analysis, combined eluates were lyophilized and reconstituted in 20 µl of 1 % formic acid. Separation of peptides by reversed-phase chromatography was carried out on an UltiMate 3000 RSLCnano System (Thermo Scientific, Dreieich) which was equipped with a C18 Acclaim Pepmap100 preconcentration column (100µm i.D.x20mm, Thermo Fisher) in front of an Acclaim Pepmap100 C18 nano column (75 µm i.d. × 150 mm, Thermo Fisher). A linear gradient of 4% to 40% acetonitrile in 0.1% formic acid over 90 min was used to separate peptides at a flow rate of 300 nl/min. The LC-system was coupled on-line to a maXis plus UHR-QTOF System (Bruker Daltonics, Bremen) via a CaptiveSpray nanoflow electrospray source (Bruker Daltonics). Data-dependent acquisition of MS/MS spectra by CID fragmentation was performed at a resolution of minimum 60000 for MS and MS/MS scans, respectively. The MS spectra rate of the precursor scan was 2 Hz processing a mass range between m/z 175 and m/z 2000. Via the Compass 1.7 acquisition and processing software (Bruker Daltonics) a dynamic method with a fixed cycle time of 3 s and a m/z dependent collision energy adjustment between 34 and 55 eV was applied. Raw data processing was performed in Data Analysis 4.2 (Bruker Daltonics), and Protein Scape 3.1.3 (Bruker Daltonics) in connection with Mascot 2.5.1 (Matrix Science) facilitated database searching of the Swiss-Prot *Homo sapiens* database (release-2020_01, 220420 entries). Search parameters were as follows: enzyme specificity trypsin with 1 missed cleavage allowed,

precursor tolerance 0.02 Da, MS/MS tolerance 0.04 Da, carbamidomethylation or propionamide modification of cysteine, oxidation of methionine, deamidation of asparagine and glutamine were set as variable modifications. Mascot peptide ion-score cut-off was set 15. If necessary, fragment spectra were validated manually. Protein list compilation was done using the Protein Extractor function of Protein Scape.

Metabolite analysis by gas chromatography – mass spectrometry

Intermediates of glycolysis and TCA cycle were analyzed by gas chromatography coupled to mass spectrometry (GC-MS). To harvest the cells for analysis, the cell culture supernatant was removed and cells were washed three times with phosphate-buffered saline (PBS) and then scrapped with cold 80% methanol. The suspension was collected, the cell culture dish was washed with 80 % methanol and the combined sample was stored at −80 °C.

For further sample preparation, the sample suspension was thawed and 10 µL of an aqueous internal standard mix containing stable isotope labeled analogs of the analytes was added. The sample was vortexed, and centrifuged (9560 g, 5min, 4 °C). The supernatant was collected and the pellet was resuspended twice in 200 µL 80% methanol with in-between supernatant collection. The last wash was centrifuged at a higher speed (13800 g). All supernatants were combined and dried in a vacuum evaporator (CombiDancer, Hettich AG, Bach, Switzerland). Sample residues were dissolved in 100 µL pure water and an aliquot was transferred into a flat bottom insert in a 1.5-mL glass vial. The aliquot was evaporated to dryness and then subjected to methoximation and silylation for GC-MS analysis using the derivatization protocol and instrumental setup previously described (Dettmer et al., 2011). A Rxi-5ms column (30m, 0.25mm ID, 0.25µm film thickness, Restek, Bad Homburg Germany) with a 2-m guard column was used. The temperature program started at 50 °C (0.5 min), followed by a ramp of 5°C/min to 120 °C, then 8 °C/min to 300 °C, and the final temperature was held for 5 min. The carrier gas was helium with a flow rate of 0.7 mL/min. The mass spectrometer was operated in full scan mode with a scan range of 50 to 550 m/z. An injection volume of 1 µL with splitless injection at 280°C was used.

For analysis of cell culture supernatants, 10 µL of the supernatant and 10 µL of the aqueous internal standard mix were transferred into a flat bottom insert in a 1.5-mL glass vial, dried and subjected to derivatization and GC-MS analysis as described.

Quantification was performed using calibration curves based on the area ratio of the endogenous compound to the stable isotope labeled standard (Mass Hunter Quantitative Analysis, version B.07.01/build 7.1.524.0, Agilent Technologies). Data were normalized to total protein. Protein amount was determined using a fluorescence assay as recently described (Berger et al., 2021).

^{35}S-methionine metabolic labelling of mitochondrial proteins

In order to label newly synthesized mitochondrially expressed proteins, the previously published protocol was used (Pearce et al., 2017). Briefly, cells at approximately 80% confluency were incubated in methionine/cysteine-free medium for 10 min before the medium was replaced with methionine/cysteine-free medium containing 10% dialyzed FCS and emetine dihydrochloride (100 μg/ml) to inhibit cytosolic translation. Following a 20 min incubation, 120 μCi/ml of [^{35}S]-methionine (Perkin Elmer) was added and the cells were incubated for 30 min. After washing with PBS, cells were lysed, and 30 μg of protein was loaded on 10–20% Tris- glycine SDS-PAGE gels. Dried gels were visualized with a PhosphorImager system.

Ribosome Profiling of Mitochondria

Cells were grown in T-75 flasks to 70% confluence in DMEM media and METTL8 overexpression was induced with 2 μg/mL of doxycycline 24 hours prior to collection. Cells were washed once with ice cold PBS, flash frozen on liquid nitrogen and stored at -80°C until lysis. 667 μL of 1.5x Lysis buffer (30 mM Tris–HCl pH 7.8, 150 mM KCl, 15 mM $MgCl_2$, 1.5 mM DTT, 1.5% triton X-100, 0.15% NP40, 1× complete phosphatase and protease inhibitors) was added to each flask and cells were collected with a cell scraper while flasks thawed on an ice slurry. ~1 mL of lysate was transferred to a chilled 1.5 mL tube, gently passed through a 27-gauge needle 10 times, and spun at 5,000G for 10 minutes at 4°C. Digestion was carried out by adding 1,500 U of MNase, 10 μL of SUPErase•In, and $CaCl_2$ to a final concentration of 5mM to 400 μL of lysate and incubating at 22°C for 1 hour. Digestion was stopped by adding EGTA to a final concentration of 6 mM. Lysate was loaded onto a 5-30% sucrose gradient (20mM Tris–HCl pH 7.8, 100 mM KCl, 10 mM $MgCl_2$, and 1 mM DTT and spun for 2.5 hrs at 40,000 rpm in an SW40 rotor. The 55S mitoribosome fraction was collected using a BioComp Fractionator. Footprints were isolated through SDS/hot phenol/chloroform extraction.

Following each step, footprints or PCR products were cleaned by either Zymo's Oligo Clean and Concentrator or DNA Clean and Concentrator, respectively. Small RNAs were size selected using the Purelink miRNA isolation kit. 3' ends were dephosphorylated with NEB Quick CIP and 3' adapter ligation was carried out with Rnl2(1-249)K227Q ligase over night at 4°C. 3' adapter: 5'-rAppNNTGACTGTGGAATTCTCGGGTGCCAAGG-L, where the underlined sequence is the library barcode. Barcoded footprint libraries were then combined and phosphorylated by PNK. Footprints were then ligated to a 5' DNA-RNA adapter with RNA Ligase. 5'(aminolinker)GTTCAGAGTTCTACAGTCCGACGATCrNrNrNrN. Reverse transcription was carried out with SuperScript IV. RT Primer GCCTTGGCACCCGAGAATTCCA. Libraries were initially amplified by PCR using the RT primer and a short 5' primer, CTTCAGAGTTCTACAGTCCGACGA. Footprints were size selected by a Pippen Prep, 3% C gel. Sizes of 74-94 were selected, corresponding to footprint sizes of 15-35. Libraries were then amplified with long indexing primers and sequenced.

Ribosome profiling analysis

Deduplicated reads were mapped to a chrM transcriptome based on the hg38 genome. P site positioning was determined by Plastid, measuring from the start codons of ND4 and ATP6. Changes in relative ribosomal occupancy was measured by first determining the proportion of ribosome density at each codon relative to the total density in the encompassing gene. Then fold change is then calculated dividing the relative ribosomal density at each position in the experimental dataset by the WT control.

pLOGO analysis

pLOGO (O'Shea et al., 2013) backgrounds were the E, P, and A site sequences of all codons that had ribosomal density in both the experimental and control datasets. Foregrounds were defined as the E, P, and A sites that had a fold change greater than 2.

QUANTIFICATION AND STATISTICAL ANALYSIS

Please refer to the Figure Legends or the Experimental Details for description of sample size and statistical analyses.

Excel-format supplemental table:

Table S1: Table of used oligonucleotides described in the STAR Methods, related to STAR Methods.

References

Alexandrov, A., Martzen, M.R., and Phizicky, E.M. (2002). Two proteins that form a complex are required for 7-methylguanosine modification of yeast tRNA. RNA *8*, 1253-1266.

Alshammari, M.A., Alshammari, T.K., and Laezza, F. (2016). Improved Methods for Fluorescence Microscopy Detection of Macromolecules at the Axon Initial Segment. Front Cell Neurosci *10*, 5.

Anderson, S., Bankier, A.T., Barrell, B.G., de Bruijn, M.H., Coulson, A.R., Drouin, J., Eperon, I.C., Nierlich, D.P., Roe, B.A., Sanger, F., *et al.* (1981). Sequence and organization of the human mitochondrial genome. Nature *290*, 457-465.

Anderson, S., de Bruijn, M.H., Coulson, A.R., Eperon, I.C., Sanger, F., and Young, I.G. (1982). Complete sequence of bovine mitochondrial DNA. Conserved features of the mammalian mitochondrial genome. J Mol Biol *156*, 683-717.

Arimbasseri, A.G., Iben, J., Wei, F.Y., Rijal, K., Tomizawa, K., Hafner, M., and Maraia, R.J. (2016). Evolving specificity of tRNA 3-methyl-cytidine-32 (m3C32) modification: a subset of tRNAsSer requires N6-isopentenylation of A37. RNA *22*, 1400-1410.

Balacco, D.L., and Soller, M. (2019). The m(6)A Writer: Rise of a Machine for Growing Tasks. Biochemistry *58*, 363-378.

Barros, M.H., and McStay, G.P. (2020). Modular biogenesis of mitochondrial respiratory complexes. Mitochondrion *50*, 94-114.

Begik, O., Lucas, M.C., Liu, H., Ramirez, J.M., Mattick, J.S., and Novoa, E.M. (2020). Integrative analyses of the RNA modification machinery reveal tissue- and cancer-specific signatures. Genome Biol *21*, 97.

Berger, R.S., Wachsmuth, C.J., Waldhier, M.C., Renner-Sattler, K., Thomas, S., Chaturvedi, A., Niller, H.H., Bumes, E., Hau, P., Proescholdt, M., *et al.* (2021). Lactonization of the Oncometabolite D-2-Hydroxyglutarate Produces a Novel Endogenous Metabolite. Cancers (Basel) *13*.

Bohnsack, M.T., and Sloan, K.E. (2018a). The mitochondrial epitranscriptome: the roles of RNA modifications in mitochondrial translation and human disease. Cell Mol Life Sci *75*, 241-260.

Bohnsack, M.T., and Sloan, K.E. (2018b). Modifications in small nuclear RNAs and their roles in spliceosome assembly and function. Biol Chem *399*, 1265-1276.

Cabello-Villegas, J., Winkler, M.E., and Nikonowicz, E.P. (2002). Solution conformations of unmodified and A(37)N(6)-dimethylallyl modified anticodon stem-loops of Escherichia coli tRNA(Phe). J Mol Biol *319*, 1015-1034.

Chen, H., Gu, L., Orellana, E.A., Wang, Y., Guo, J., Liu, Q., Wang, L., Shen, Z., Wu, H., Gregory, R.I., *et al.* (2020). METTL4 is an snRNA m(6)Am methyltransferase that regulates RNA splicing. Cell Res.

Chujo, T., and Tomizawa, K. (2021). Human transfer RNA modopathies: diseases caused by aberrations in transfer RNA modifications. FEBS J.

Delaunay, S., and Frye, M. (2019). RNA modifications regulating cell fate in cancer. Nat Cell Biol *21*, 552-559.

Desrosiers, R., Friderici, K., and Rottman, F. (1974). Identification of methylated nucleosides in messenger RNA from Novikoff hepatoma cells. Proc Natl Acad Sci U S A *71*, 3971-3975.

Dettmer, K., Nurnberger, N., Kaspar, H., Gruber, M.A., Almstetter, M.F., and Oefner, P.J. (2011). Metabolite extraction from adherently growing mammalian cells for metabolomics studies: optimization of harvesting and extraction protocols. Anal Bioanal Chem *399*, 1127-1139.

Dominissini, D., Moshitch-Moshkovitz, S., Schwartz, S., Salmon-Divon, M., Ungar, L., Osenberg, S., Cesarkas, K., Jacob-Hirsch, J., Amariglio, N., Kupiec, M., *et al.* (2012). Topology of the human and mouse m6A RNA methylomes revealed by m6A-seq. Nature *485*, 201-206.

Doxtader, K.A., Wang, P., Scarborough, A.M., Seo, D., Conrad, N.K., and Nam, Y. (2018). Structural Basis for Regulation of METTL16, an S-Adenosylmethionine Homeostasis Factor. Mol Cell *71*, 1001-1011 e1004.

Ganichkin, O.M., Anedchenko, E.A., and Wahl, M.C. (2011). Crystal structure analysis reveals functional flexibility in the selenocysteine-specific tRNA from mouse. PLoS One *6*, e20032.

Goh, Y.T., Koh, C.W.Q., Sim, D.Y., Roca, X., and Goh, W.S.S. (2020). METTL4 catalyzes m6Am methylation in U2 snRNA to regulate pre-mRNA splicing. Nucleic Acids Res *48*, 9250-9261.

Han, L., and Phizicky, E.M. (2018). A rationale for tRNA modification circuits in the anticodon loop. RNA *24*, 1277-1284.

Hao, Z., Wu, T., Cui, X., Zhu, P., Tan, C., Dou, X., Hsu, K.W., Lin, Y.T., Peng, P.H., Zhang, L.S., *et al.* (2020). N(6)-Deoxyadenosine Methylation in Mammalian Mitochondrial DNA. Mol Cell *78*, 382-395 e388.

Ignatova, V.V., Jansen, P., Baltissen, M.P., Vermeulen, M., and Schneider, R. (2019). The interactome of a family of potential methyltransferases in HeLa cells. Sci Rep *9*, 6584.

Ignatova, V.V., Kaiser, S., Ho, J.S.Y., Bing, X., Stolz, P., Tan, Y.X., Lee, C.L., Gay, F.P.H., Lastres, P.R., Gerlini, R., *et al.* (2020a). METTL6 is a tRNA m(3)C methyltransferase that regulates pluripotency and tumor cell growth. Sci Adv *6*, eaaz4551.

Ignatova, V.V., Stolz, P., Kaiser, S., Gustafsson, T.H., Lastres, P.R., Sanz-Moreno, A., Cho, Y.L., Amarie, O.V., Aguilar-Pimentel, A., Klein-Rodewald, T., *et al.* (2020b). The rRNA m(6)A methyltransferase METTL5 is involved in pluripotency and developmental programs. Genes Dev.

Kazuhito, T., and Wei, F.Y. (2020). Posttranscriptional modifications in mitochondrial tRNA and its implication in mitochondrial translation and disease. J Biochem *168*, 435-444.

Ke, S., Pandya-Jones, A., Saito, Y., Fak, J.J., Vagbo, C.B., Geula, S., Hanna, J.H., Black, D.L., Darnell, J.E., Jr., and Darnell, R.B. (2017). m6A mRNA modifications are deposited in nascent pre-mRNA and are not required for splicing but do specify cytoplasmic turnover. Genes Dev *31*, 990-1006.

Knuckles, P., Carl, S.H., Musheev, M., Niehrs, C., Wenger, A., and Buhler, M. (2017). RNA fate determination through cotranscriptional adenosine methylation and microprocessor binding. Nat Struct Mol Biol *24*, 561-569.

Kweon, S.M., Chen, Y., Moon, E., Kvederaviciute, K., Klimasauskas, S., and Feldman, D.E. (2019). An Adversarial DNA N(6)-Methyladenine-Sensor Network Preserves Polycomb Silencing. Mol Cell *74*, 1138-1147 e1136.

Lamichhane, T.N., Mattijssen, S., and Maraia, R.J. (2013). Human cells have a limited set of tRNA anticodon loop substrates of the tRNA isopentenyltransferase TRIT1 tumor suppressor. Mol Cell Biol *33*, 4900-4908.

Lee, Y., Choe, J., Park, O.H., and Kim, Y.K. (2020). Molecular Mechanisms Driving mRNA Degradation by m(6)A Modification. Trends Genet *36*, 177-188.

Lin, S., Liu, Q., Lelyveld, V.S., Choe, J., Szostak, J.W., and Gregory, R.I. (2018). Mettl1/Wdr4-Mediated m(7)G tRNA Methylome Is Required for Normal mRNA Translation and Embryonic Stem Cell Self-Renewal and Differentiation. Mol Cell *71*, 244-255 e245.

Liu, J., Yue, Y., Han, D., Wang, X., Fu, Y., Zhang, L., Jia, G., Yu, M., Lu, Z., Deng, X., *et al.* (2014). A METTL3-METTL14 complex mediates mammalian nuclear RNA N6-adenosine methylation. Nat Chem Biol *10*, 93-95.

Marchand, V., Ayadi, L., Ernst, F.G.M., Hertler, J., Bourguignon-Igel, V., Galvanin, A., Kotter, A., Helm, M., Lafontaine, D.L.J., and Motorin, Y. (2018). AlkAniline-Seq: Profiling of m(7) G and m(3) C RNA Modifications at Single Nucleotide Resolution. Angew Chem Int Ed Engl *57*, 16785-16790.

Mendel, M., Chen, K.M., Homolka, D., Gos, P., Pandey, R.R., McCarthy, A.A., and Pillai, R.S. (2018). Methylation of Structured RNA by the m(6)A Writer METTL16 Is Essential for Mouse Embryonic Development. Mol Cell *71*, 986-1000 e1011.

Meyer, K.D., Saletore, Y., Zumbo, P., Elemento, O., Mason, C.E., and Jaffrey, S.R. (2012). Comprehensive analysis of mRNA methylation reveals enrichment in 3' UTRs and near stop codons. Cell *149*, 1635-1646.

Minczuk, M., He, J., Duch, A.M., Ettema, T.J., Chlebowski, A., Dzionek, K., Nijtmans, L.G., Huynen, M.A., and Holt, I.J. (2011). TEFM (c17orf42) is necessary for transcription of human mtDNA. Nucleic Acids Res *39*, 4284-4299.

Murphy, F.V.t., Ramakrishnan, V., Malkiewicz, A., and Agris, P.F. (2004). The role of modifications in codon discrimination by tRNA(Lys)UUU. Nat Struct Mol Biol *11*, 1186-1191.

O'Shea, J.P., Chou, M.F., Quader, S.A., Ryan, J.K., Church, G.M., and Schwartz, D. (2013). pLogo: a probabilistic approach to visualizing sequence motifs. Nat Methods *10*, 1211-1212.

Pearce, S.F., Rorbach, J., Van Haute, L., D'Souza, A.R., Rebelo-Guiomar, P., Powell, C.A., Brierley, I., Firth, A.E., and Minczuk, M. (2017). Maturation of selected human mitochondrial tRNAs requires deadenylation. Elife *6*.

Pendleton, K.E., Chen, B., Liu, K., Hunter, O.V., Xie, Y., Tu, B.P., and Conrad, N.K. (2017). The U6 snRNA m(6)A Methyltransferase METTL16 Regulates SAM Synthetase Intron Retention. Cell *169*, 824-835 e814.

Rorbach, J., Bobrowicz, A., Pearce, S., and Minczuk, M. (2014). Polyadenylation in bacteria and organelles. Methods Mol Biol *1125*, 211-227.

Schiffers, S., Ebert, C., Rahimoff, R., Kosmatchev, O., Steinbacher, J., Bohne, A.V., Spada, F., Michalakis, S., Nickelsen, J., Muller, M., *et al.* (2017). Quantitative LC-MS Provides No Evidence for m(6) dA or m(4) dC in the Genome of Mouse Embryonic Stem Cells and Tissues. Angew Chem Int Ed Engl *56*, 11268-11271.

Scholler, E., Weichmann, F., Treiber, T., Ringle, S., Treiber, N., Flatley, A., Feederle, R., Bruckmann, A., and Meister, G. (2018). Interactions, localization, and phosphorylation of the m(6)A generating METTL3-METTL14-WTAP complex. RNA *24*, 499-512.

Sledz, P., and Jinek, M. (2016). Structural insights into the molecular mechanism of the m(6)A writer complex. Elife *5*.

Slobodin, B., Han, R., Calderone, V., Vrielink, J., Loayza-Puch, F., Elkon, R., and Agami, R. (2017). Transcription Impacts the Efficiency of mRNA Translation via Co-transcriptional N6-adenosine Methylation. Cell *169*, 326-337 e312.

Suzuki, T. (2021). The expanding world of tRNA modifications and their disease relevance. Nat Rev Mol Cell Biol.

Suzuki, T., Nagao, A., and Suzuki, T. (2011). Human mitochondrial tRNAs: biogenesis, function, structural aspects, and diseases. Annu Rev Genet *45*, 299-329.

Suzuki, T., and Suzuki, T. (2014). A complete landscape of post-transcriptional modifications in mammalian mitochondrial tRNAs. Nucleic Acids Res *42*, 7346-7357.

Suzuki, T., Yashiro, Y., Kikuchi, I., Ishigami, Y., Saito, H., Matsuzawa, I., Okada, S., Mito, M., Iwasaki, S., Ma, D., *et al.* (2020). Complete chemical structures of human mitochondrial tRNAs. Nat Commun *11*, 4269.

Tataranni, T., Agriesti, F., Ruggieri, V., Mazzoccoli, C., Simeon, V., Laurenzana, I., Scrima, R., Pazienza, V., Capitanio, N., and Piccoli, C. (2017). Rewiring carbohydrate catabolism differentially affects survival of pancreatic cancer cell lines with diverse metabolic profiles. Oncotarget *8*, 41265-41281.

Van Haute, L., Hendrick, A.G., D'Souza, A.R., Powell, C.A., Rebelo-Guiomar, P., Harbour, M.E., Ding, S., Fearnley, I.M., Andrews, B., and Minczuk, M. (2019). METTL15 introduces N4-methylcytidine into human mitochondrial 12S rRNA and is required for mitoribosome biogenesis. Nucleic Acids Res *47*, 10267-10281.

van Tran, N., Ernst, F.G.M., Hawley, B.R., Zorbas, C., Ulryck, N., Hackert, P., Bohnsack, K.E., Bohnsack, M.T., Jaffrey, S.R., Graille, M., *et al.* (2019). The human 18S rRNA m6A methyltransferase METTL5 is stabilized by TRMT112. Nucleic Acids Res *47*, 7719-7733.

Varshney, U., Lee, C.P., and RajBhandary, U.L. (1991). Direct analysis of aminoacylation levels of tRNAs in vivo. Application to studying recognition of Escherichia coli initiator tRNA mutants by glutaminyl-tRNA synthetase. J Biol Chem *266*, 24712-24718.

Wang, P., Doxtader, K.A., and Nam, Y. (2016a). Structural Basis for Cooperative Function of Mettl3 and Mettl14 Methyltransferases. Mol Cell *63*, 306-317.

Wang, X., Feng, J., Xue, Y., Guan, Z., Zhang, D., Liu, Z., Gong, Z., Wang, Q., Huang, J., Tang, C., *et al.* (2016b). Structural basis of N(6)-adenosine methylation by the METTL3-METTL14 complex. Nature *534*, 575-578.

Warda, A.S., Kretschmer, J., Hackert, P., Lenz, C., Urlaub, H., Hobartner, C., Sloan, K.E., and Bohnsack, M.T. (2017). Human METTL16 is a N(6)-methyladenosine (m(6)A) methyltransferase that targets pre-mRNAs and various non-coding RNAs. EMBO Rep *18*, 2004-2014.

Weixlbaumer, A., Murphy, F.V.t., Dziergowska, A., Malkiewicz, A., Vendeix, F.A., Agris, P.F., and Ramakrishnan, V. (2007). Mechanism for expanding the decoding capacity of transfer RNAs by modification of uridines. Nat Struct Mol Biol *14*, 498-502.

Xu, L., Liu, X., Sheng, N., Oo, K.S., Liang, J., Chionh, Y.H., Xu, J., Ye, F., Gao, Y.G., Dedon, P.C., *et al.* (2017). Three distinct 3-methylcytidine (m3C) methyltransferases modify tRNA and mRNA in mice and humans. J Biol Chem *292*, 14695-14703.

Zhang, L.H., Zhang, X.Y., Hu, T., Chen, X.Y., Li, J.J., Raida, M., Sun, N., Luo, Y., and Gao, X. (2020). The SUMOylated METTL8 Induces R-loop and Tumorigenesis via m3C. iScience *23*, 100968.

Zhang, L.S., Liu, C., Ma, H., Dai, Q., Sun, H.L., Luo, G., Zhang, Z., Zhang, L., Hu, L., Dong, X., *et al.* (2019). Transcriptome-wide Mapping of Internal N(7)-Methylguanosine Methylome in Mammalian mRNA. Mol Cell *74*, 1304-1316 e1308.

Zhou, K.I., Shi, H., Lyu, R., Wylder, A.C., Matuszek, Z., Pan, J.N., He, C., Parisien, M., and Pan, T. (2019). Regulation of Co-transcriptional Pre-mRNA Splicing by m(6)A through the Low-Complexity Protein hnRNPG. Mol Cell *76*, 70-81 e79.

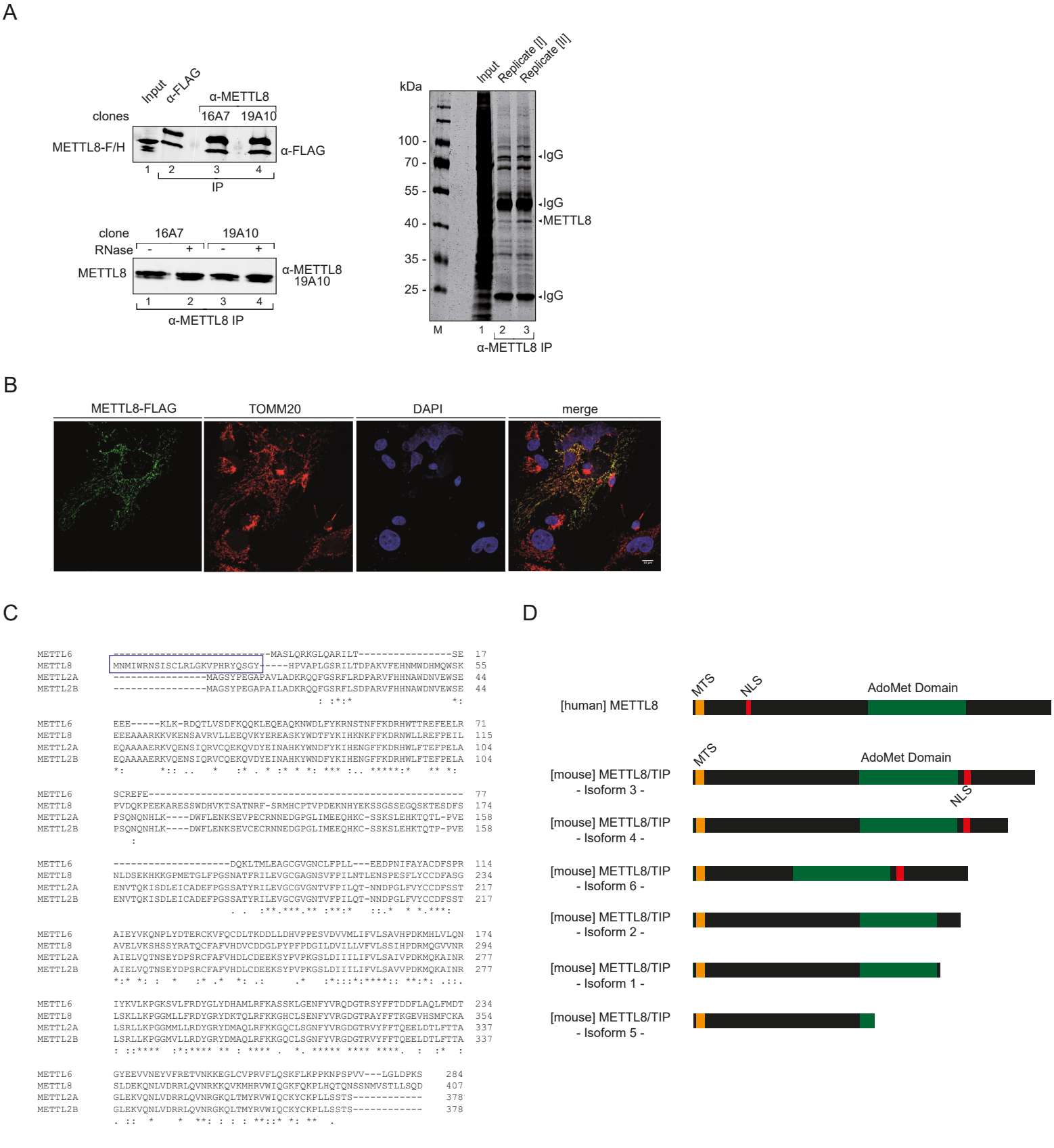

Suppl. Figure 1 related to Figure 1: METTL8 is a mitochondrially localized protein.

(A) Validation of the two METTL8 monoclonal antibody clones 16A7 and 19A10 in Flp-In TREx293 and HeLa S3 cells. Upper western blot shows IP of METTL8-F/H. IP with α-Flag antibody was used as control. Endogenous METTL8 IP is shown in the lower western blot. Lysate was treated with and without RNase I. Coomassie Blue gel on the right shows METTL8 enrichment after α-METTL8 IP in HeLa S3 cells. Lysate was purified by a sucrose gradient before. Indicated METTL8 protein was validated by LC-MS/MS analysis. (B) Immunofluorescence detection of a FLAG-tagged METTL8 construct (green), mitochondrial import receptor subunit TOM20 (red), and DAPI (blue) in HeLa cells (scale bar: 10 μm) (C) Partial sequence alignment of human METTL2A (Q96IZ6), METTL2B (Q6P1Q9), METTL6 (Q8TCB7) and METTL8 (B3KW44). Predicted mitochondrial targeting signal highlighted in blue box.

(D) Schematics of human and murine METTL8 protein domains. Conserved GxGxG S-Adenosyl-Methionine binding site highlighted in green, predicted mitochondrial targeting signal (MTS) in orange and predicted nuclear localization signal (NLS) in red. Protein schematics for human METTL8 based on B3KW44, murine METTL8 isoforms on A2AUU0.

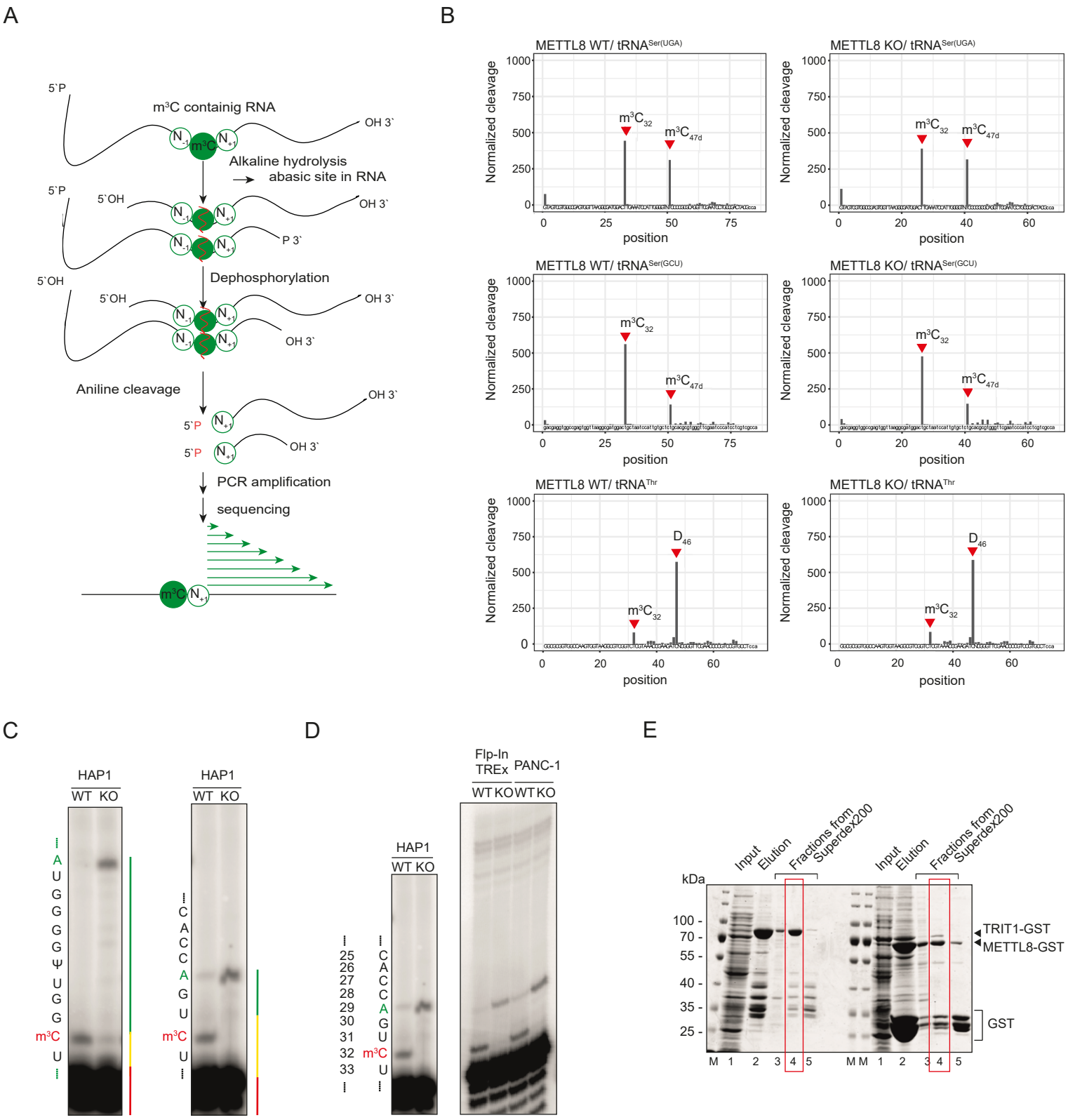

Suppl. Figure 2 related to Figure 3: METTL8 methylates position C_{32} in mt-tRNA$^{Ser(UCN)}$ and mt-tRNA^{Thr}.
(A) Illustration of the AlkAniline-Seq protocol starting with RNA strand cleavage induced by alkaline hydrolysis. After aniline cleavage of the a-basic site and primer ligation at the nucleotide N_{+1}, N_{+1} reads are enriched by sequencing strategy. m^{3}C modification is represented as a green dot, a-basic site as broken dot. (B) AlkAniline-Seq analysis of Flp-In TREx293 METTL8 WT and METTL8 KO cell lines. Left panel shows m^{3}C cleavage profile of the cytoplasmic tRNA$^{Ser\ (UGA/GCU)}$ and tRNA^{Thr} in METTL8 WT cell line. Right panel shows the corresponding m^{3}C cleavage profiles in METTL8 KO cell line. (C) Coloured bars next to each blot represent annealed [^{32}P]-radiolabelled primer in red, extension product to C_{32} shown in orange, and extension beyond C_{32} and stalling at the next adenosine due to the absence of dTTP in HAP1 cells for mt-tRNA$^{Ser(UCN)}$ (left) and mt-tRNA^{Thr} (right). The nucleotide sequence of the tRNA, corresponding to stalling events at each position, is shown to the side of the panel. (D) Verification of the m^{3}C modification on mt-tRNAThr in HAP1, PANC-1 and Flp-In TREx293 cell lines by [^{32}P]-radiolabelled primer extension. The stalling events at position C_{32} (red) and A_{29} (green) are shown to the side of the gel. (E) Recombinant TRIT1-GST and METTL8-GST protein is shown after each single purification. Protein used for analysis is marked in red.

A

Gene	MT-ND1	MT-ND2	MT-ND3	MT-ND4	MT-ND4L	MT-ND5	MT-ND6
TCA	8	7	1	9	3	13	2
TCT	2	4	0	5	0	2	3
TCC	8	11	4	17	4	21	0
TCG	0	1	0	1	1	1	0
ACA	14	11	2	22	1	18	2
ACT	1	5	1	8	1	8	2
ACC	20	23	4	15	3	26	0
ACG	0	2	0	1	0	1	0

Gene	MT-COI	MT-COII	MT-COIII	MT-ATP6	MT-ATP8	MT-CYB
TCA	7	4	7	4	2	14
TCT	7	1	2	4	0	0
TCC	9	4	7	2	1	11
TCG	1	0	0	0	1	0
ACA	15	8	11	10	2	13
ACT	4	5	2	3	1	4
ACC	11	8	11	12	4	13
ACG	2	0	0	0	1	1

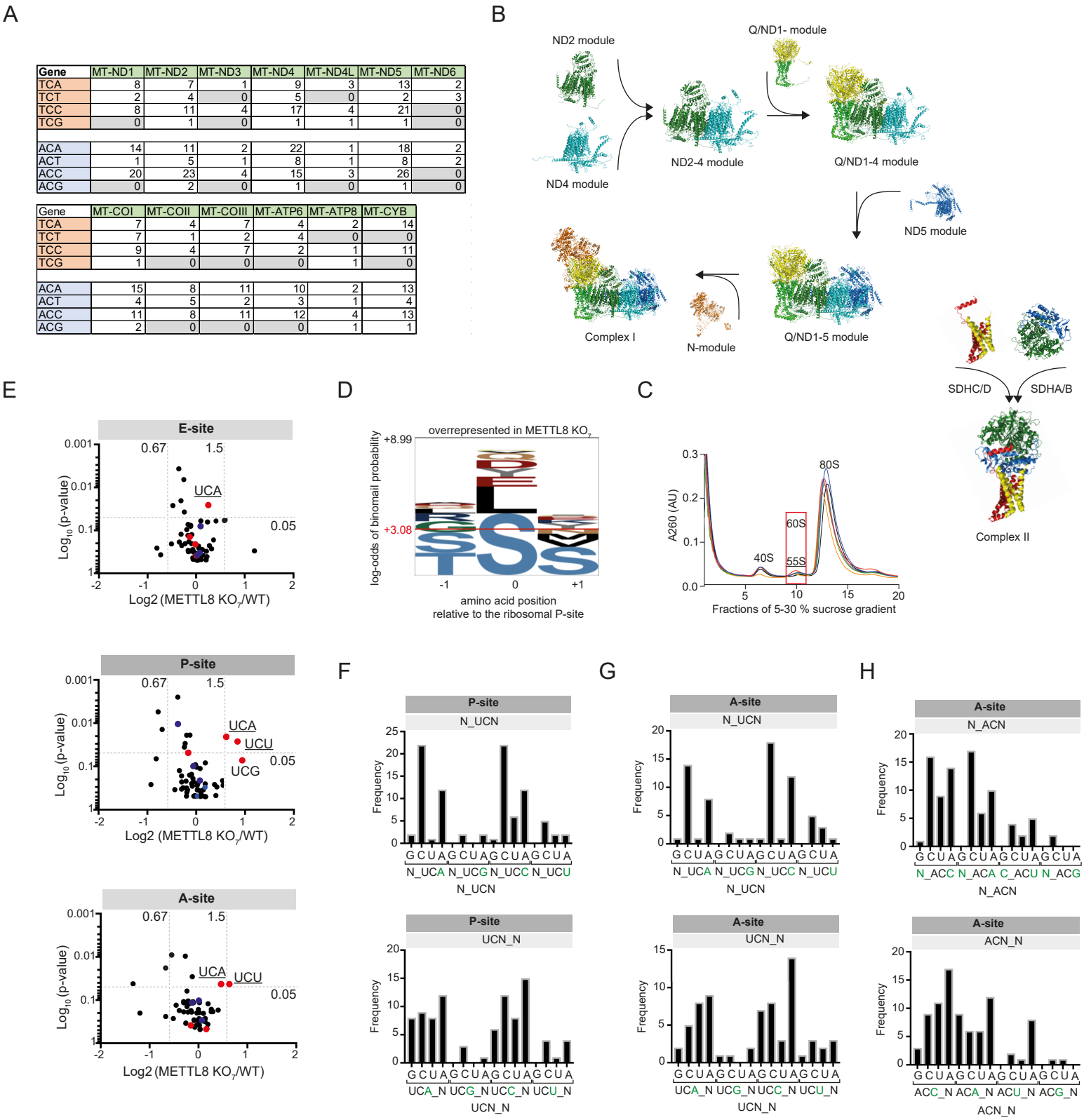

Suppl. Figure 3 related to Figure 7: m^3C_{32} unbalancing in mt-tRNA$^{Ser(UCN)}$ and mt-tRNA^{Thr} affects translation dynamics and respiratory complex assembly.

(A) Codon distribution of mt-tRNASer$^{(UCN)}$ (red) and mt-tRNA^{Thr} (blue) among all 13 mitochondrial encoded genes. Codons not available in a gene highlighted in grey. (B) Complex I (lower panel) and complex II (upper panel) assembly model based on (Barros and McStay, 2020; Sanchez-Caballero et al., 2016; Signes and Fernandez-Vizarra, 2018). Crystal structures (PDB ID: 1zoy; 5ldw) were downloaded from PDB and modified in Pymol. (C) Ribosome footprinting of Flp-In TREx METTL8 WT, METTL8 KO and METTL8 overexpressing cell lines. MNase treated ribosomes separated by sucrose density centrifugation and intact monosomes were isolated. (D) Amino acid overrepresentation at positions relative to the P-site in an independent Flp-In TREx293 METTL8 KO clone. Horizontal red line indicates significantly overrepresentation. (E) Ribosomal redistribution in E-, P- and A-site of an independent Flp-In TREx293 METTL8 KO clone based on the codon. Red dots represent mt-tRNA$^{Ser(UCN)}$ codons, mt-tRNA^{Thr} codons are highlighted in blue. Significant overrepresented codons are underlined. (F) Frequency of mt-tRNA$^{Ser(UCN)}$ quadruplets in the P-site. Frequency of mt-tRNA$^{Ser(UCN)}$ codons with an additional upstream nucleotide (N_UCN) is shown in the right panel. Left panel shows frequency of mt-tRNA$^{Ser(UCN)}$ codons with an additional downstream nucleotide (UCN_N). (G) Frequency of mt-tRNA$^{Ser(UCN)}$ quadruplets in the A-site. Frequency of mt-tRNA$^{Ser(UCN)}$ codons with an additional upstream nucleotide (N_UCN) is shown in the right panel. Left panel shows frequency of mt-tRNA$^{Ser(UCN)}$ codons with an additional downstream nucleotide (UCN_N). (H) Frequency of mt-tRNA^{Thr} quadruplets in the A-site. Frequency of mt-tRNA^{Thr} codons with an additional upstream nucleotide (N_ACN) is shown in the right panel. Left panel shows frequency of mt-tRNA^{Thr} codons with an additional upstream nucleotide (ACN_N).

KEY RESOURCES TABLE

REAGENT or RESOURCE	SOURCE	IDENTIFIER
Antibodies		
Mouse monoclonal anti-HA.11 antibody (clone 16B2)	Covance	Cat# MMS-101P, RRID:AB_2314672
Mouse monoclonal anti-beta actin antibody (ab6276)	Abcam	Cat# ab6276, RRID:AB_2223210
Mouse monoclonal anti-GAPDH (GT239)	GeneTEx	Cat# GTX627408, RRID:AB_11174761
Mouse monoclonal anti-p54[nrb]	BD Transduction Laboratories	Cat# 611278, RRID:AB_398806
Mouse monoclonal anti-FLAG®M2 (F3165)	Sigma	Cat# F3165, RRID:AB_259529
Rabbit polyclonal anti-TOM20 (FL-145)	Santa Cruz Biotechnologies	Cat# sc-11415, RRID:AB_2207533
Goat polyclonal anti-mouse IgG, IRDye 800CW conjugated antibody	LI-COR Bioscience	Cat#925-32210; RRID: AB_2687825
Goat polyclonal anti-rabbit IgG, IRDye 800CW conjugated antibody	LI-COR Bioscience	Cat#926-32211; RRID: AB_621843
Rat monoclonal anti-METTL8 antibody (clone 16A7)	this paper	N/A
Rat monoclonal anti-METTL8 antibody (clone 19A10)	this paper	N/A
Bacterial and virus strains		
Escherichia coli Rosetta™ (DE3) competent cells	Novagen	Cat#70954-3
XL1 blue competent cells	this paper	N/A
Chemicals, peptides, and recombinant proteins		
METTL8 (22-407 aa.) – GST (human)	this paper	N/A
TRIT1 (22-467 aa.) – GST (human)	this paper	N/A
OVA-METTL8 peptide	Peps4LS, Heidelberg	N/A
Thermostable inorganic pyrophosphatase	New England BioLabs®	Cat#M0296
RNA T7 Polymerase	this paper	N/A
T4 Polynucleotide Kinase (T4 PNK)	Thermo Fisher Scientific	Cat#EK0031
Antarctic phosphatase	New England BioLabs®	Cat#M0289S
RiboLock RNase Inhibitor	Thermo Fisher Scientific	Cat#EO0384
ProteinaseK	AppliChem	Cat#A3830
ProteinaseK	Thermo Fisher Scientific	Cat#AM2546
Blasticidin	Gibco	Cat#A1113903
Zeocin	Invitrogen	Cat#R25001
Hygromycin B	Invitrogen	Cat#10687010
Tetracycline	AppliChem	Cat#A2228.0025
Penicillin/ Streptomycin	Sigma	Cat#P0781
AEBSF	Sigma Aldrich	Cat#A8456
Digitonin	Merck	Cat#300410
Glutamate	Sigma Aldrich	Cat#G1626
Malate	Sigma Aldrich	Cat#M1000
ADP	Calbiochem	Cat#11705
Cytochrome *c*	Sigma Aldrich	Cat#C7752
Succinate	Sigma Aldrich	Cat#S2378
Oligomycin	Sigma Aldrich	Cat#O4876
FCCP	Sigma Aldrich	Cat#C2920

Rotenone	Sigma Aldrich	Cat#8875
Antimycin	Sigma Aldrich	Cat#A6874
Aprotinin	Roche	N/A
Emetine dihydrochloride	Calbiochem	Cat#324693
Incomplete Freund's adjuvant (IFA)	Helmholtz Center Munich	N/A
Lipofectamin™ 2000	Invitrogen	Cat#11668500
Fibronectin Solution (Bovine)	Sigma Aldrich	Cat#F1141
Collagen solution from calf skin	Sigma Aldrich	Cat#C8918
Ham`s F12 Nutrient Mixture	Thermo Fisher Scientific	Cat#11765054
Poly-D lysine	Sigma Aldrich	Cat#P6407
Crystal Violet	Sigma Aldrich	Cat#HT90132
MitoTracker™ Deep Red FM	Invitrogen	Cat#M22426
Hoechst 33342	Thermo Fisher Scientific	Cat#H1399
Coomassie Brilliant Blue R250	BioRad	Cat#1610436
γ,γ-Dimethylallyl pyrophosphate (DMAPP)	Sigma Aldrich	Cat#38426
EDC (1-ethyl-3-(3-dimethylaminopropyl) - carbodiimide hydrochloride)	Sigma Aldrich	Cat#E7750; CAS: 25952-53-8
1-Methylimidazole	Sigma-Aldrich	Cat#M50834; CAS: 616-47-7
CPG oligonucleotide	Tib Molbiol, Berlin	N/A
γ-^{32}P-ATP	Hartmann Analytic	Cat#FP-501
[^{3}H] S-Adenosyl-L-Methionine	Hartmann Analytic	Cat#ART2008
[^{35}S]-methionine	Perkin Elmer	Cat# NEG009A005MC
Scintillations Cocktail	Zinsser Analytic	N/A
illustra™ MicroSpin G-25 column	GE Healthcare	Cat#27532501
Glutathione Sepharose™ 4 FastFlow	GE Healthcare	Cat#17-5132-02
Superdex™ 200 10/30 GL	GE Healthcare	Cat#17-5175-01
Protein G Sepharose slurry	GE Healthcare	Cat#17061801
ANTI-FLAG M2 Affinity Gel	Sigma Aldrich	Cat#A2220
Phenol/Chloroform/Isoamylalcohol	Roth	Cat#A156.1
TRIzol	Invitrogen	Cat#15596018
Critical commercial assays		
Phusion® High-Fidelity DNA Polymerase	New England BioLabs®	Cat#M0530L
NucleoSpin Gel and PCR Clean-up kit	Macherey-Nagel	Cat#740609.50
NucleoSpin Mini Plasmid, Mini kit	Macherey-Nagel	Cat#740588.50
NucleoBond Xtra Midi EF, Midi kit	Macherey-Nagel	Cat#740422.50
MiSeq reagent Kit V3 (150 cycles)	Illumina	Cat#MS-102-3001
SuperScript™ III First-Strand Synthesis System	Invitrogen	Cat#18080400
T4 DNA Ligase kit	Thermo Fisher Scientific	Cat#EL0011
First-strand cDNA synthesis kit	Thermo Fisher Scientific	Cat#K1612
Takyon™ No ROX SYBR 2x MasterMix blue dTTP	Eurogentec	Cat#NA.55
T4 Polynucleotide Kinase (T4 PNK) kit – Buffer B	Thermo Fisher Scientific	Cat#EK0031
Next Small RNA kit	New England BioLabs®	Cat#E7330S/L
SERVA*Gel*™ Native Gel Starter Kit	Serva	Cat#43204.1
Deposited data		
Alk-Aniline-Seq	this paper	ENA: PRJEB45091
mitoRibosome Profiling	this paper	GEO:GSE180400

Orginal western and northern blots	this paper	https://data.mendeley.com//datasets/47kvzxmgkg/1
Experimental models: Cell lines		
Human: Flp-In™TREx™ -293	ATCC	Cat# CRL-1573, RRID:CVCL_0045
Human: Flp-In™TREx™ -293 METTL8 -/- clone C12_05	this paper	N/A
Human: Flp-In™TREx™ -293 METTL8 -/- clone C07_05	this paper	N/A
Human: Flp-In™TREx™ -293 METTL8-F/H	this paper	N/A
Human: Flp-In™TREx™ -293 METTL8-F/H D230A	this paper	N/A
Human: Flp-In™TREx™ -293 F7H-METTL2	this paper	N/A
Human: PANC-1	ATCC	Cat# 300228/p635_Panc-1, RRID:CVCL_0480
Human: PANC-1 METTL8 -/- clone C13_13	this paper	N/A
Human: PANC-1 METTL8 -/- clone C13-24	this paper	N/A
Human: CAPAN-1	ATCC	Cat# 300143/p663_Capan-1, RRID:CVCL_0237
Human: A-549	ATCC	Cat# A549, RRID:CVCL_0023
Human: HAP1	Horizon Discovery	RRID:CVCL_Y019
Human: HAP1 METTL8 -/-	Horizon Discovery	RRID:CVCL_SY13
Human: HeLa	ATCC	Cat# CCL-2, RRID:CVCL_0030
Human: HeLa S3	ATCC	Cat# 300384/p699_HeLa_S3, RRID:CVCL_0058
P3X63Ag8.653 myeloma cells	ATCC	ATCC Cat# CRL-8008, RRID:CVCL_4032
Oligonucleotides		
DNA oligonucleotide for strand-specific cDNA-synthesis, see Table 1 for a list of oligonucleotides	Metabion	N/A
DNA oligonucleotide for mt-mRNA RIP by qPCR, see Table 1 for a list of oligonucleotides	Metabion	N/A
Northern blot probe sequences, see Table 1 for a list of oligonucleotides	Metabion	N/A
DNA oligonucleotide sequences for cloning and mutagenesis, see Table 1 for a list of oligonucleotides	Metabion	N/A
DNA oligonucleotide sequences for mt-tRNA *in vitro* transcription, see Table 1 for a list of oligonucleotides	Metabion	N/A
Recombinant DNA		
pcDNA™5/FRT/TO modified with N-terminal F/H-tag	Invitrogen	Cat#V652020
pOG44	Invitrogen	Cat#V600520
pcDNA™5/FRT/TO METTL8-F/H	this paper	N/A
pcDNA™5/FRT/TO METTL8-F/H D230A	this paper	N/A
pcDNA™5/FRT/TO METTL8-F/H I4Q	this paper	N/A
pcDNA™5/FRT/TO METTL8-F/H I4/9Q	this paper	N/A
pcDNA™5/FRT/TO METTL8-F/H I4/9 L12Q	this paper	N/A
pcDNA™5/FRT/TO F/H-METTL2	this paper	N/A
pX459 sgRNA METTL8	this paper	N/A

pcDNA5/FRT/TO METTL8 FLAG.STREP2-tag	this paper	N/A
pIRES-VP5 modified	Meister et al.,2004	N/A
pIRES-VP5 METTL8-EGFP	this paper	N/A
pIRES-VP5 METTL8-EGFP I4Q	this paper	N/A
pIRES-VP5 METTL8-EGFP I4/6Q	this paper	N/A
pIRES-VP5 METTL8-EGFP I4/9 L12Q	this paper	N/A
pIRES-VP5 F/H-METTL2	this paper	N/A
pIRES-VP5 F/H-METTL8-F/H	this paper	N/A
pETM14 TRIT1-GST	this paper	N/A
pETM14 METTL8-GST	this paper	N/A
Software and algorithms		
Quantity One Software	BioRad	Quantity One 1-D Analysis Software, RRID:SCR_014280
Data Analysis 4.2	Bruker Daltonics	N/A
Protein Scape 3.1.3	Bruker Daltonics	N/A
Mascot 2.5.1	Matrix Science	RRID: SCR_014322
Protein Scape	Bruker Daltonics	N/A
Uniprot		UniProtKB, RRID:SCR_004426
PyMOL		PyMOL, RRID:SCR_000305
Odyssey	LI-CORE	Odyssey CLx, RRID:SCR_014579
Zen10 Microscope Software	Zeiss	N/A
DatLab	Oroboros Instruments	Product ID: 20700
RCSB Protein Data Bank (PDB)		RCSB PDB), RRID:SCR_012820
MitoFates	http://mitf.cbrc.jp/MitoFates/cgi-bin/top.cgi	
Clustal Omega	https://www.ebi.ac.uk/Tools/msa/clustalo/	
PrimerX	http://www.bioinformatics.org/primerx/	
NCBI database		NCBI, RRID:SCR_006472
pLOGO		pLogo, RRID:SCR_018185
Other		
LSM 710, AxioObserver microscope with a C-Apochromat 63x/1.20 W Korr M27 objective	Zeiss	N/A
Zeiss Axiovert200M microscope	Zeiss	N/A
Multimode-Microplate reader Mithras LB 940	Berthold Technologies	N/A
CFX96real-Time System BioRad	BioRad	N/A
Personal Molecular Imager™ System	BioRad	N/A
Multipurpose Scintillation Counter	Beckmann Coulter LS6500	N/A
Potter S Homogenizer	B. Braun Biotech International	N/A
UltiMate 3000 RSLCnano System	Thermo Fisher Scientific	N/A
C18 Acclaim Pepmap100 preconcentration column	Thermo Fisher Scientific	N/A

Acclaim Pepmap100 C18 nano column	Thermo Fisher Scientific	N/A
maXis plus UHR-QTOF System	Bruker Daltonics	N/A
CaptiveSpray nanoflow electrospray source	Bruker Daltonics	N/A